J Extreme Events, Vol. 2, No. 2 (2015) 1550007 (46 pages)

DOI: 10.1142/S2345737615500074

World Scientific
www.worldscientific.com

Regional Variation of Transient Precipitation and Rainless-day Frequency Across a Subcontinental Hydroclimate Gradient

Daniel A. Bishop* and Neil Pederson
Harvard University
324 N Main Street, Petersham, MA 01366, USA
**dbishop@fas.harvard.edu*

Published 17 December 2015

Extreme daily and transient precipitation events have been on the rise in the continental United States. These changes have the potential to disrupt human and natural systems. Tree rings can reconstruct annual estimates of past climate, but have limitations in reconstructing extreme precipitation events. We analyzed instrumental records to evaluate patterns in daily, weekly, and seasonal precipitation in four regions spanning a climatic gradient in the eastern United States. Relationships between tree-ring reconstructions of hydroclimate and precipitation events were analyzed to characterize extreme years over the last 1000 years. From 1944–2013, the Hudson Valley and Ohio Valley regions have experienced wetter summers as well as an increase in the frequency of daily rainfall. Coinciding with these increases, half or more of the extreme wet years in these two regions have occurred in the last 20 years. Significant differences in the structure of weekly growing-season precipitation between extreme wet and dry years were found in late May and late June in the Ohio Valley and early June in the Mississippi Valley, with negligible differences in the northern and southern ends of our gradient. We also found dry-spell duration was significantly different between extreme wet and dry years in all regions except for the northern end of our study gradient. In contrast, dry-spell frequency was significantly different between extreme wet and dry years in all regions except for the southern end of our gradient. Reconstructed Palmer Drought Severity Index (PDSI) was significantly and positively correlated with total summer rainfall and significantly and negatively correlated with rainless-day frequency in all regions, with stronger correlations during extreme years. Working in the region with the strongest relations, we reconstructed summer precipitation and summer rainless days in the Hudson Valley back to 1525 CE and 1625 CE, respectively. From these reconstructions, we infer that the 20th century is characterized by more extreme summer precipitation totals and a decline in rainless days with 75.8% of the last 33 years having fewer dry days than the 377-year mean. The forecasted changes toward

*Corresponding author.

longer, more intense droughts over the next century are not yet realized in our study regions. However, should these shifts occur, human and natural systems will likely undergo abrupt change in response to alterations in hydrology, ecological disturbance, and terrestrial productivity, with the Northeast potentially being most vulnerable.

Keywords: Climate change; extreme events; paleoclimatology; drought; pluvial; dendrochronology; forest ecology; reconstruction; hydroclimatology.

1. Introduction

Global climate change is expected to have a significant impact on the occurrence, seasonality, intra-season variability, and intensity of precipitation. Extreme transient precipitation events (e.g., high intensity precipitation, high number of days without rainfall) have been on the rise in the continental United States (Kunkel *et al.* 2003; Kunkel 2003; Easterling *et al.* 2000; Singh *et al.* 2013; Villarini *et al.* 2013). Recent impact assessments help evaluate changes in climate extremes under a known period of climate change, which have shown an increase in precipitation and heavy precipitation events in the eastern US since the mid-20th century (DeGaetano 2009; Peterson *et al.* 2008). These recent increases are projected to continue in North America through the end of the 21st century (IPCC 2014), the impacts of which are expected to be significant for human and natural systems.

Reflecting broader patterns of increased precipitation over much of the US since 1900 (Melillo *et al.* 2014), there has been an increase in streamflow and water table height across the northeastern US, leading to higher risks of flood in the region (Weider and Boutt 2010). Interestingly, in the Midwestern US, there has been an increase in the number of floods, but not an increase in the size of these floods (Mallakpour and Villarini 2015). However, under projected increases in temperature from climate change, reductions in days with precipitation and increases in dry-spell length are anticipated in many regions across the globe (Giorgi *et al.* 2011). Terrestrial ecosystems are particularly vulnerable through anticipated increases in soil water stress and heavy evaporative losses (IPCC 2014). Extreme moisture fluctuations have been thought to trigger forest dieback, specifically under severe fluctuations in hydroclimate from high intensity rainfall to prolonged drought (Auclair 1993). Some of these fluctuations have been documented in many forests around the world (Allen *et al.* 2010). In addition, more frequent, long-duration droughts have been thought to reduce tree response to precipitation pulses, suggesting there will be increased potential for forest mortality given current climate projections (Plaut *et al.* 2013). Understanding the frequency, timing, and spatial extent of different classes of extreme climatic and weather events is particularly important to avoid

loss of life and to prevent increasing economic and monetary costs associated with catastrophic extreme events (Karl and Easterling 1999). There is a growing need to add to our understanding of hydroclimatic regimes across the eastern US as the temporal and spatial distributions of precipitation regimes change over time.

Instrumental climate records are relatively short and can often only characterize climate at multi-annual to decadal time scales. Proxies of past climate, including those that reconstruct precipitation, effective moisture, lake levels, and inferred soil moisture, can characterize climate from centuries to millennia. Some of these proxies are: pollen (Bartlein *et al.* 2011; Viau *et al.* 2006), sedimentary records (Hubeny *et al.* 2011; Newby *et al.* 2014), stable isotopes (West *et al.* 2006), and tree rings (Cook and Krusic 2004; Cook *et al.* 2004; Stahle *et al.* 2007; Cleaveland *et al.* 2011; Pederson *et al.* 2013). In the Northeast US, two of these proxies indicate that all but one of the most intense droughts of the last 500–1000 years occurred prior to the observational record (Hubeny *et al.* 2011; Pederson *et al.* 2013), making it critical to understand hydroclimatic dynamics prior to the instrumental record. Of these proxies, tree rings can provide a unique perspective, acting as a strong annual, and even seasonal (e.g., earlywood and latewood), proxy of climate (Fritts 1976, 1991), offering a finer temporal scale for paleoclimate data. Identifying the relation between instrumental records of extreme events and tree-ring records could yield a more concrete understanding of the frequency of extreme events over centuries.

Drought is often characterized in terms of cumulative moisture at seasonal and annual temporal scales. However, transient moisture availability is also important to ecology. One index of a transient climate, the number of "rainless" days (defined in climatology as a full day with < 1 mm of measurable liquid water equivalent of precipitation), combines with precipitation event intensity to play a key role in changing regional precipitation regimes (Polade *et al.* 2014). Regional rainless-day frequency and variability have been investigated in different areas of the world (Lucero and Rozas 2002; Brunetti *et al.* 2001). In the eastern United States, the frequency of rainless days is projected to increase during the 21st century (Singh *et al.* 2013), which coincides with an increase in the daily intensity and frequency of intense rainfall events over the northeast United States (Thibeault and Seth 2014). Such a combination may lead to alternating hydroclimatic extremes (Singh *et al.* 2013), which can challenge the resiliency of ecosystems. Summer, a season of frequent heightened drought stress on trees in the northern hemisphere (Williams *et al.* 2010; St. George and Ault 2014), is particularly important in temperate terrestrial ecosystems with regards to tree survival and ecosystem productivity (Holst *et al.* 2008).

Here we use instrumental records to evaluate seasonal trends in rainless-day frequency and dry-spell duration as well as frequency across four regions in the contiguous eastern United States (Figure 1). We chose two regions experiencing contrasting trends and patterns in precipitation. The Hudson Valley of southeastern NY State is currently experiencing a significant shift in increased precipitation and extreme events (Seager *et al.* 2012; Pederson *et al.* 2013; Matonse and Frei 2013). At the other extreme, the ecotone of the western edge of the eastern deciduous forest and southern Great Plains in Texas and Oklahoma is experiencing a severe drought that follows one of the wettest centuries since the 1500s (Cleaveland *et al.* 2011). We include two additional regions between the Hudson Valley and Southern Plains to better investigate a gradient of moisture regimes within a transect experiencing opposing changes in hydroclimate.

Based on strong relationships between instrumental summer precipitation and summer rainless days with an existing reconstruction of Palmer Drought Severity Index (PDSI) in the Hudson Valley, we use the Hudson Valley tree-ring network to reconstruct these two instrumental variables to characterize extreme years of reconstructed PDSI in terms of total precipitation and rainless-day frequency over the last 500 years. Because a new reconstruction of precipitation was recently developed for the Hudson Valley (Tipton *et al.* 2015), we focus our paleoclimatic results on the rainless-day reconstruction. Our results have both climatological and ecological implications for the eastern United States.

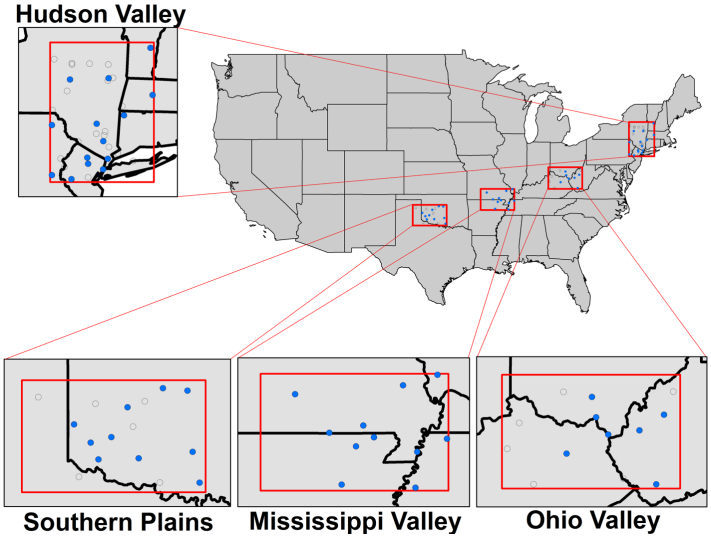

Figure 1. US Historical Climatology Stations Across Four Study Regions in the Eastern Contiguous US. Stations that Met Selection Criteria are in Blue and those that did not are Hollow Circles

2. Methods

2.1. *Study regions and observational records*

For our four regions of study, bounding boxes were established for Hudson Valley (40.5–43.5 N, 72.5–75.5 W), Ohio Valley (37.5–39.5 N, 81–85 W), Mississippi Valley (35.5–37.5 N, 89–93 W), and Southern Plains (34–36 N, 97–101 W) regions. Similar-sized areas were selected for the Mississippi Valley and Ohio Valley regions to maintain spatial consistency and provide a relatively continuous moisture availability gradient. Observational records of daily precipitation and temperature (maximum and minimum) were selected from the US Historical Climatology Network (USHCN, Williams *et al.* 2006) within each region using two quality control criteria: (1) stations with $>90\%$ daily coverage from 1944–2013 to evaluate adequacy of each station, and (2) 95% daily representation in each given 3-month season (Winter DJF, Spring MAM, Summer JJA, and Fall SON) to evaluate adequacy of each individual season and year in the analysis. USHCN stations that failed to meet criterion (1) were entirely removed from the analysis. However, individual seasons from a given year that did not meet criterion (2) were removed but did not disqualify the station from contributing data from other seasons or years that met the same criterion. Using this approach, some stations were permitted to contribute data to certain years but not to others. From the potential pool of daily records in each region, 14 stations qualified in the Hudson Valley, 7 in the Ohio Valley, 11 in the Mississippi Valley, and 10 in the Southern Plains regions (Figure 1). We did not employ any data correction processes to address missing days due to the conservative nature of our quality-control criteria. Data availability is summarized by season in Table S1 and Figure S1 in the online supplementary material.

2.2. *Data analysis*

Reconstructed PDSI, an estimate of soil moisture availability developed from the strong relationship between instrumental PDSI and tree-ring chronologies, for each region was downloaded from the North American Drought Atlas (NADA) (Cook and Krusic 2004; Cook *et al.* 2008); for details on reconstructed PDSI see "*Development of paleoclimate from tree rings*" below. Reconstructions of PDSI for the Ohio Valley, Mississippi Valley, and Southern Plains regions ended in 2005 CE, while the Hudson Valley from Pederson *et al.* (2013) ended in 2011 CE. Averaged instrumental summer (JJA) PDSI values for recent years were also derived from the National Climatic Data Center's online database (www.ncdc.noaa.gov/; Vose *et al.* 2013) and added to the end of each region's reconstruction. The Hudson Valley region was represented by New York (Divisions 2, 4, 5, and 6),

Massachusetts (Division 1), Connecticut (Division 1), Pennsylvania (Division 1), and New Jersey (Division 1); the Ohio Valley region was represented by Ohio (Divisions 8 and 9), Kentucky (Divisions 3 and 4), and West Virginia (Division 3); the Mississippi Valley region was represented by Arkansas (Divisions 2 and 3) and Missouri (Divisions 5 and 6); and the Southern Plains region was represented by Oklahoma (Divisions 4, 5, and 7). Mean summer PDSI was averaged across all divisions for each region.

Seasonal precipitation was calculated for each season as a sum of all daily precipitation for each individual observational record, and then averaged annually for each region. Rainless days here are defined as "climatological" rainless days: 24 h periods with less than or equal to 1 mm of precipitation and calculated as a frequency for each season across all observational records. We also tested other definitions of rainless days: "trace" (0.25 mm limit) and "absolute" (0 mm limit). Lastly, we calculated mean daily rainfall (mean precipitation "intensity") as the summer precipitation divided by the number of days with measurable rainfall (> 1 mm). We calculated trends for regionally averaged seasonal precipitation, rainless-day frequency, and mean daily rainfall using the non-parametric Theil–Sen slope (Sen 1968) to estimate the linear rate of change for 1944–2013. The Mann–Kendall tau trend test was used as a significance test to evaluate directionality in each time series (Kendall 1938), and is reported as the *p*-value for Theil–Sen slopes for the remainder of this paper.

In addition to linear trend analysis, we fit kernel density functions to four distinct periods during 1944–2013: (1) full period, 1944–2013; (2) early period, 1944–1973; (3) late period, 1974–2013; and (4) most recent 20 years, 1994–2013. The most recent period was chosen as an extra, targeted period to capture the recent accelerated increase in extreme hydrological events and moisture availability since the mid-1990s observed by Matonse and Frei (2013) and Pederson *et al.* (2013), respectively. Kernel density functions were calculated for all individual station rainless-day frequencies (not averaged) within each region using the "density" function in R (R Development Core Team 2012). This approach enabled a multi-dimensional evaluation of changes in the means and spread of rainless-day frequency. We used the two-sample, two-tailed Kolmogorov–Smirnov test (Massey 1951) to evaluate the significance of the changes in rainless-day frequencies.

Next, to evaluate the nonlinear relationship between drought reconstructions and rainfall, we calculated Spearman's rank correlation coefficients (Spearman 1904) for regional PDSI with both regionally averaged rainless days and total precipitation for the summer season. We also calculated a second set of statistics on a more extreme set of values. First, we calculated Spearman rank correlations on

reconstructed PDSI less than -1 and greater than $+1$ for 1944–2013 versus the number of rainless days for those years. Second, to test the differences in temporal structure of daily rainfall for the summer with opposite extremes of moisture availability, we calculated a moving 7-day window sum of daily precipitation for years with reconstructed PDSI greater than $+2$ (extreme wet years) and years with reconstructed PDSI less than -2 (extreme dry years). We then calculated a simple difference (wet minus dry years). The significance and consistency of the differences in weekly precipitation totals between extreme years were evaluated using bootstrap resampling, tallying the proportion of simulations ($n = 1000$) with non-overlapping 99.9% confidence intervals. Resampling was performed using a random number generator to randomly select observed weekly precipitation data from station data in each region with replacement, producing a new dataset with the same sample size for each simulation.

To evaluate the effects of dry spells in each region, we calculated summer frequencies and durations of dry spells using the instrumental daily precipitation data. A "dry-spell" was defined as a period of time greater than or equal to five days that did not include a single day with measured precipitation above 1 mm. To account for dry spells that began earlier than the first day of June and end after the last day of August, dry spells were calculated between May 1st and September 30th for each year. Mean dry-spell duration was then calculated as the average length of dry spells for each year. The Kruskal–Wallis rank sum test (Kruskal and Wallis 1952), a non-parametric analysis of variance (ANOVA) test, was performed to test for significant differences between extreme wet and dry years in each of these two dry-spell variables. All analysis up to this point was completed using R (R Development Core Team 2012).

2.3. *Development of paleoclimate from tree rings*

The NADA is a product-ready spatial and temporal reconstruction of drought history (Cook and Krusic 2004; Cook *et al.* 2008). Reconstructions of drought used in this study were derived from hundreds of collections of living and dead tree samples (Cook *et al.* 2007). Each sample was visually crossdated (Stokes and Smiley 1968). That is, a hypothesized calendar year was assigned for each ring on each sample based upon the pattern of large and small rings through time within each collection. Once visual crossdating was found to be satisfactory for samples within a collection, each ring was measured to the nearest 0.01–0.001 mm. Visual crossdating of each measured ring was statistically verified using the program COFECHA (Holmes 1983). If the hypothesized dates passed statistical testing, each chronology, the average time-series from all samples in a collection, was

considered provisionally crossdated. Final dating was confirmed when each chronology was compared to independent chronologies of the same species in the same region, though it is possible to verify dating across species in some cases. Once the rigorous steps of crossdating are completed, authors of these data can be confident that they have a time-series of ring widths where extreme events can be precisely dated to a specific calendar year. It is this basic step of dendrochronology that allows investigators to identify and understand historical extreme events in climatic and ecological systems.

Because geometric and ecological factors impart low-frequency trends and abrupt changes in ring widths that are not related to climate, crossdated time-series of ring widths are not ready for reconstruction of climate until they are detrended. The goal of detrending for reconstructions of climate is to separate as much of the geometric and ecological "noise" from the climatic signal as possible (Douglass 1919; Fritts 1976; Cook and Kairiukstis 1990). Particularly, an important aim of detrending is to retain as much low frequency trend as possible to determine long-term trends in climate (e.g., Jacoby and D'Arrigo 1989). One broad limitation on retaining low frequency in tree rings is the length of the segment from which measurements are derived, the so-called "segment-length curse" (Cook *et al.* 1995). In closed-canopy forests like those in the eastern US, another limitation of retaining low-frequency trends comes as the result of changes in tree-to-tree competition (Cook and Peters 1981). For the tree-ring based reconstruction here, we follow the standardization of Pederson *et al.* (2004), where if there were no abrupt changes observed in individual time-series of raw radial increment from trees in closed-canopy forests, detrending was conducted using a straight-line fit to retain all possible low-frequency information. Ultimately, detrending develops a time-series of dimensionless and standardized chronology tree-ring indices.

A suite of monthly or seasonal climatic indices (e.g., precipitation, temperature, drought indices) is the common target for climatic reconstructions. The variables that correlate strongly with the standardized tree-ring chronologies, often based upon a hypothesis when determining a sampling location, are used to calibrate the reconstruction (Cook *et al.* 1996, 1999). A common reconstruction of moisture availability is the average summer PDSI. For our work here, we used the standard procedure in the creation of a tree-ring based climate reconstruction (Cook *et al.* 1999) for total rainfall and total number of rainless days during the summer (June, July, August) in the Hudson Valley region. Compared to the other regions, total precipitation and rainless-day frequencies in the Hudson Valley region exhibited the strongest relationship with reconstructed PDSI, leading us to conclude that it was the best example to demonstrate how climate is reconstructed from tree-ring chronologies.

Using a principal component approach to reconstruct past climate from tree rings (Cook *et al.* 1999), a model of the relationship between standardized tree-ring chronologies and total summer precipitation and the number of summer rainless days was calibrated on the last two-thirds of the instrumental data for the common period between the tree rings and instrumental data and verified by the remaining first third of the common period. Typically, calibration-verification is conducted on one-half of the common period. We reasoned that with the relatively short period of overlap between rainless days and tree rings, 1944–1981, we would use a 2/3rd–1/3rd calibration-verification approach for model development. Since carbon gained through photosynthesis in prior years can be allocated for tree growth (Trumbore *et al.* 2002; Kagawa *et al.* 2006; Carbone *et al.* 2013), ring widths in a given year can be influenced by climate in both the current and prior year. Thus, we used current and prior year growth as predictors of total summer precipitation and summer rainless days, which led to a total of 84 potential predictors from 42 tree-ring chronologies for each example reconstruction (Table S2 in the online supplementary material). Only predictors with a positive correlation to total precipitation and a negative correlation to rainless days at the $p \leq 0.05$ level entered the calibration model. The calibration model was then verified against the remaining data. If the coefficient of efficiency and reduction of error statistics are positive, the calibration model is generally considered to have skill in back-casting climate history (Cook *et al.* 2007).

Because the potential predictors in our reconstruction — the tree-ring chronologies — had different lengths, we used a nested approach in developing hydroclimate history for the Hudson Valley (Meko 1997; Cook *et al.* 2003). We stepped back in 25-year nests after making the first reconstruction from the common period nest of 1836–1981 CE. That is, the first backwards nest following the common period only contained chronologies with data between 1800 and 1981 CE. We continued to step back in 25-year nests until the coefficient of efficiency or reduction of error dropped below zero. Because the instrumental records we used have data until 2013, we made forward nests using recently collected tree-ring records so that we could use as much tree-ring data as possible for our reconstruction. In this case, we made two forward nests until they failed or dropped in replication to less than four records. All reconstructed nests were normalized and then combined such that only unique periods for each nest were added to the common nest; data predating the common period of all chronologies, 1800–1836, were then added to the common nest. Once the normalized reconstruction was stitched together, each normalized time-series was multiplied by the standard deviation of the instrumental data. Following this, the mean of the instrumental total summer precipitation and total summer rainless days was added to each

reconstruction and then multiplied by the standard deviation of the instrumental data so each final chronology had the same mean and range of variance as the instrumental data. Instrumental data after 2003 was then appended to the end of the reconstructed summer rainless-day frequency and after 2001 for the total summer precipitation series to bring both up to 2013 CE.

3. Results

3.1. *Regional climate, 1944–2013*

We found that the Hudson Valley and Ohio Valley were characterized by relatively cooler climates; the Mississippi Valley by a warmer, wet climate; and the Southern Plains by a warmer, dry climate (Table 1). The Hudson Valley, Ohio Valley, and Southern Plains regions all received the majority of their annual precipitation during the spring and summer months on average, with summer being the wettest on average. However, the Mississippi Valley's wettest season was spring by a large difference with other seasons. There was high interseasonal variability in precipitation in the Southern Plains region, ranging from 98.4 mm in the winter to 239.7 mm in the spring. Both summer and fall precipitation in the Hudson Valley have significantly increased ($p < 0.05$) toward wetter conditions (both 11.5 mm decade^{-1}). There were no other significant trends in total precipitation for any season in the other three regions. From 1944 to 2013, summer precipitation was significantly correlated with instrumental PDSI for all regions ($p < 0.001$). The Hudson Valley region was highest in magnitude ($\rho = 0.83$) relative to the Ohio Valley ($\rho = 0.69$), Mississippi Valley ($\rho = 0.67$), and Southern Plains ($\rho = 0.61$) regions (Figure 2). There were no significant temporal trends in mean daily summer rainfall (mm/day; mean precipitation intensity) for any region; however, there has been an increase since the mid-2000s in the Hudson Valley.

Extreme seasons of precipitation and moisture availability were evaluated using total precipitation and reconstructed PDSI (1944–2013), respectively. In most regions, a greater number of extreme high precipitation summers were found than low precipitation summers (> 2 standard deviations from the mean). Furthermore, most of these precipitation extremes have occurred in recent decades (Table 1). The majority of extremely wet PDSI years occurred after 2000 in the Hudson Valley (54%, $n = 7$), while the majority of extremely dry reconstructed PDSI years occurred in the 1960s (71%, $n = 5$). In the Ohio Valley, half of the extremely wet reconstructed PDSI years occurred after 1995 (50%, $n = 5$). The distribution of extreme years in the Mississippi Valley and Southern Plains regions were not clustered and spread relatively evenly over the records since

Table 1. Seasonal Climatology, Precipitation Trends, and Extreme PDSI Years by Region (1944–2013). Significant Precipitation Trends in **bold** ($p < 0.05$)

Region	Season	TMax (°C)	TMin (°C)	Precipitation (mm)	Precipitation Change (mm/decade)	Mann–Kendall Tau	Wet Years (> 2 SD)	Dry Years (> 2 SD)
Hudson Valley	*Winter*	2.5	−7.3	256.7	4.7	0.11	1958, 1979, 2008	1980
	Spring	14.7	2.5	304.3	1.8	0.04	1953, 1983, 1984, 2011	—
	Summer	27.2	14.8	320.7	**11.5**	**0.18**	2009, 2011, 2013	—
	Fall	16.8	5.4	305.2	**11.5**	**0.19**	1977, 2005	1964
Ohio Valley	*Winter*	6.9	−4.4	245.5	−0.4	−0.01	1950, 1979	—
	Spring	19.2	4.8	306.2	2.6	0.03	2011	—
	Summer	29.5	16.2	312.4	6.7	0.13	1958, 1979, 2003	1944, 1957
	Fall	20.2	6.3	232.3	5.4	0.10	2004, 2006, 2011	1953
Mississippi Valley	*Winter*	8.8	−2.4	294.2	4.1	0.07	1950	1963
	Spring	21.0	8.1	374.8	0.8	0.01	1945, 1973, 2008, 2011	—
	Summer	31.6	18.9	276.6	−1.5	−0.03	—	1953
	Fall	22.0	8.5	295.9	9.7	0.13	1984, 1988	1953
Southern Plains	*Winter*	11.7	−2.1	98.4	3.1	0.09	1993, 1998	—
	Spring	23.3	8.8	239.7	1.8	0.03	1957	—
	Summer	34.4	20.5	229.2	2.8	0.05	1950, 1996, 2007	—
	Fall	24.1	9.8	196.5	4.5	0.07	1986	—

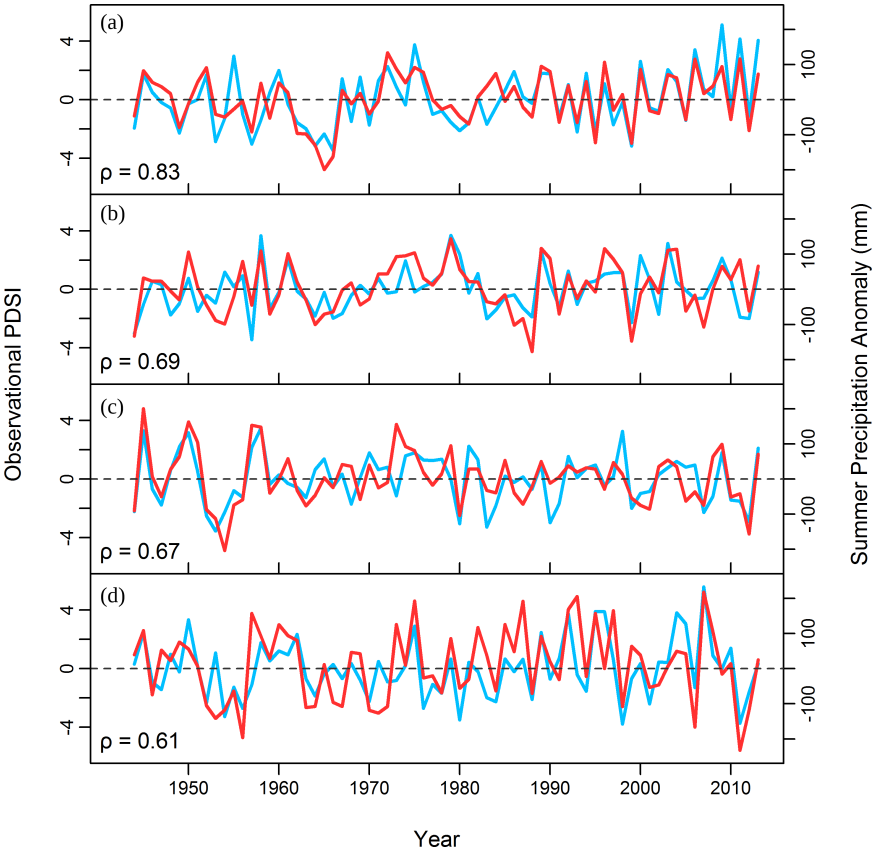

Figure 2. (Color online) Observational PDSI (red lines) and Mean Summer Precipitation Anomalies (light blue lines) for (a) Hudson Valley, (b) Ohio Valley, (c) Mississippi Valley, and (d) Southern Plains regions

1994. Importantly, instrumental PDSI was used after 1978 in the North American Drought Atlas (Cook and Krusic 2004; Cook *et al.* 2008) and after 2003 for the Hudson Valley PDSI reconstruction (Pederson *et al.* 2013). These additions to each reconstruction need to be considered carefully when evaluating results. However, in the Hudson Valley, PDSI of recent years do agree with previous work on extremes in hydroclimatic instrumental records in the region (Matonse and Frei 2013).

From 1944 to 2013, reconstructed PDSI had positive correlations with summer precipitation for all regions ($p < 0.001$). As with the instrumental PDSI correlations, the Hudson Valley region was highest in magnitude ($\rho = 0.77$) relative to the Ohio Valley ($\rho = 0.59$), Mississippi Valley ($\rho = 0.55$), and Southern Plains ($\rho = 0.53$) regions (not shown).

3.2. *Transient differences between wet and dry years*

In analyzing transient structures of rainfall and dry spells, we were able to identify temporal and static differences in dry-spell characterizations between extreme wet and dry years in each region at the weekly time step during the growing-season; a daily analysis proved to be too noisy and we extended the season of analysis one month prior to summer in the event that we ignore significant differences through an arbitrary definition of seasons. For this analysis, we base extreme wet and dry years on $+/-2$ standard deviations of reconstructed PDSI so we could gain insight into the long-term occurrence of extreme precipitation. In the Hudson Valley, weekly precipitation was consistently higher in extreme wet years versus extreme dry years throughout the summer, although bootstrap resampling ($< 50\%$) indicated no consistent significant difference between wet and dry years. In the Ohio Valley, extreme wet years had two periods with significantly greater rainfall than dry years during late May and late June, peaking at 98.6% of simulations returning significant differences in late May. In the Mississippi Valley, there was one distinct period where differences in precipitation during extreme wet years versus dry years were significantly greater in early June. In the Southern Plains, as in the Hudson Valley, precipitation was consistently higher in extreme wet years versus extreme dry years throughout the summer, but there were no weeks with significant differences between wet and dry years (Figure 3).

Dry-spell duration was significantly different between wet and dry years in all regions except the Hudson Valley ($p < 0.05$, Kruskal–Wallis ANOVA; Figure 4). In contrast, dry-spell frequency was significantly different for all regions except the Southern Plains ($p < 0.05$). These results indicate that the structure of precipitation during drought changes from northeast to southwest across the eastern US: increased frequency of dry spells is more characteristic of dry years in the northeastern end of our transect while increased duration of dry spells is more characteristic of dry years in the southwestern end.

3.3. *Trends in instrumental rainless-day frequency*

On average, the Hudson Valley and Ohio Valley had negative trends in climatological summer rainless-day frequency from 1944 to 2013, -0.47 days decade^{-1} (Mann–Kendall $p = 0.058$) and -0.46 days decade^{-1} (Mann–Kendall $p = 0.051$) for the calculated Theil–Sen slope, respectively. That is, it is raining more frequently in recent years in the Hudson and Ohio valleys than in the past. There were no significant long-term trends for the other two regions.

When varying the threshold of a "rainless day", the mean number of rainless days varied. In the Hudson Valley, there were 66.2 "climatological" rainless days

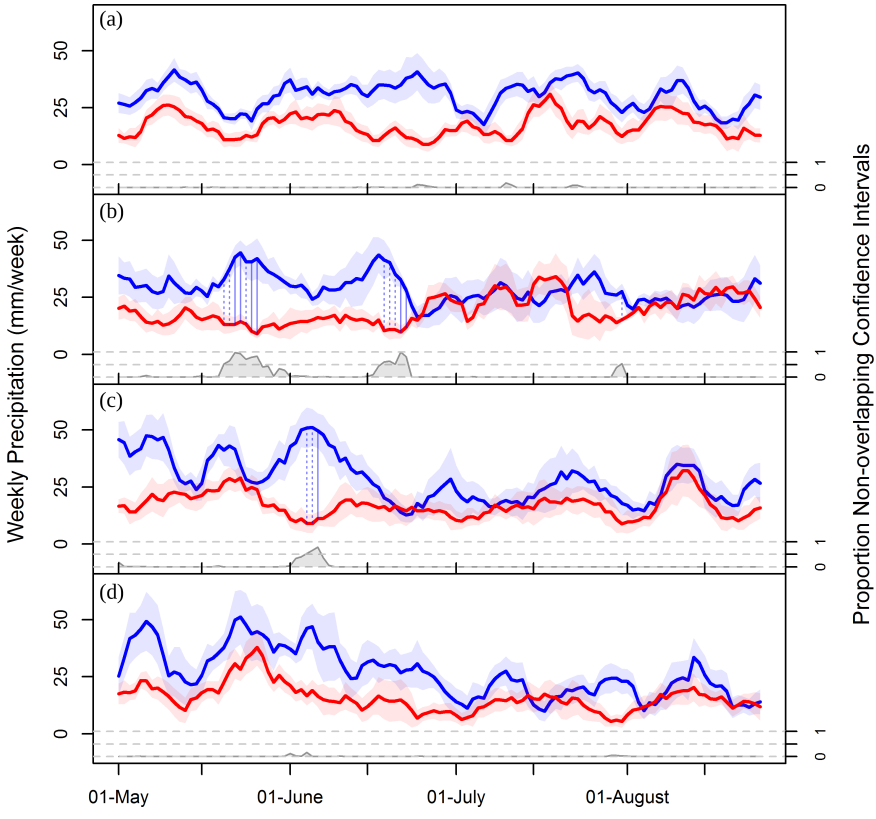

Figure 3. (Color online) Weekly Precipitation (May–August; 1944–2013) Averages for Wet Years (reconstructed Summer PDSI $> +2$; Blue Lines) and Dry Years (reconstructed summer PDSI < -2; red lines) with Bootstrapped 99.9% Confidence Intervals (shaded blue and red) in (a) Hudson Valley, (b) Ohio Valley, (c) Mississippi Valley, and (d) Southern Plains Regions.

Notes: Proportions of bootstrapped simulations at which 99.9% sample confidence intervals do not overlap are represented by gray shade at bottom. Dashed vertical blue lines indicate weeks where greater than 50% and solid vertical blue lines indicate weeks where 75% of simulations are significantly different.

out of a maximum of 92 days (∼72% of the summer), 61.5 "trace" rainless days (67%), and 52.7 "absolute" rainless days (57%). In the Ohio Valley, these values are 65.9 (72%), 62.0 (67%), and 57.5 (63%) while in the Mississippi Valley region, they are 72.5 (79%), 70.0 (76%), and 66.2 (72%), respectively. Finally, the values for these three definitions in the Southern Plains are 76.5 (83%), 74.4 (81%), and 70.4 (77%). On average, there were 13.5 summer days (∼15% of the summer) with liquid precipitation between 0 and 1 mm in the Hudson Valley, 8.4 days (9%) in the Ohio Valley, 6.3 days (7%) in the Mississippi Valley, and 6.1 (7%) in the Southern Plains (Figure 5). There were no significant changes in trace and absolute rainless

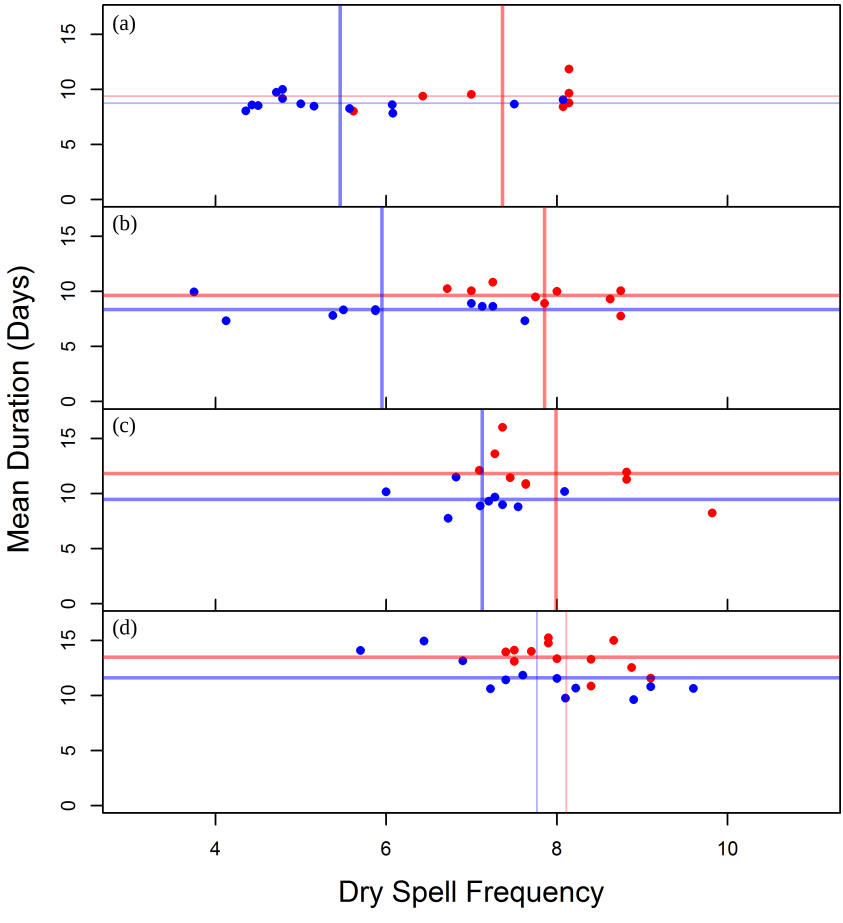

Figure 4. (Color online) Dry-spell Frequency (Number of Dry Spells) and Mean Duration for Wet Years (Reconstructed Summer PDSI $> +2$ for 1944–2013; blue points) and Dry Years (Reconstructed Summer PDSI < -2; red points) in (a) Hudson Valley, (b) Ohio Valley, (c) Mississippi Valley, and (d) Southern Plains Regions.

Notes: Transparent lines indicate means for dry-spell frequency (vertical) and mean duration (horizontal). Thick lines indicate significant differences ($p < 0.05$; Kruskal–Wallis test).

days in the Hudson Valley and Ohio Valley, although the directionality remained the same. There were no significant changes in mean rainless-day frequency for any region in the winter, fall, and spring seasons (Figures S2–S4). For the remainder of this paper, "rainless days" are defined as "climatological" rainless days (< 1 mm).

In the Hudson Valley, summer rainless-day frequencies from the most recent 20 years had significantly fewer rainless days relative to the full 1944–2013 period (Two-tailed Kolmogorov–Smirnov test $D = 0.13$, $p < 0.05$) (Figure 6(a)). The

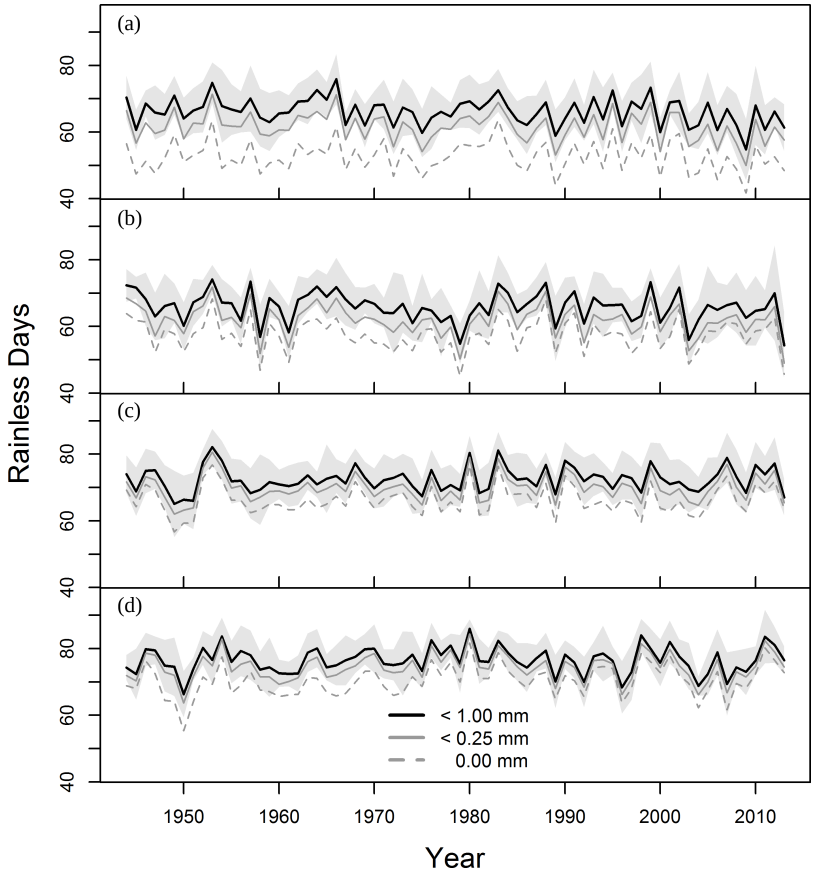

Figure 5. Mean Summer Rainless-day Frequencies (1944–2013) for (a) Hudson Valley, (b) Ohio Valley, (c) Mississippi Valley, and (d) Southern Plains Regions.
Notes: Rainless-day frequencies plotted across three thresholds: < 1 mm (solid black lines), < 0.25 mm (solid gray lines), and 0 mm (dashed gray lines). 95% confidence interval (gray shading) is included for rainless-day frequencies < 1 mm only.

same change toward fewer rainless days was observed in the Ohio Valley, although it was insignificant using traditional thresholds of significance testing ($D = 0.12$, $p = 0.08$) (Figure 6(b)). No significant changes were observed in the Mississippi Valley or Southern Plains regions (Figures 6(c) and 6(d)). In the density functions of both the Hudson Valley and Ohio Valley summer rainless days, a flattening relative to the full period is apparent for the most recent 20 years. That is, a widening of the distribution (increased variance, larger range) is apparent. There were some notable changes in other seasons, as well. In the fall, Ohio Valley rainless-day frequencies from the most recent 20 years had significantly more rainless days relative to the full period ($D = 0.13$, $p < 0.05$). The winter density

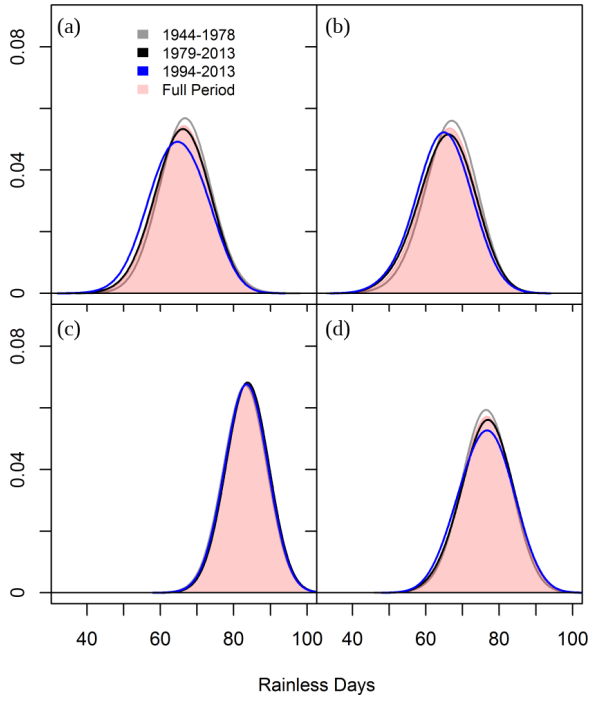

Figure 6. (Color online) Kernel Density Functions of Summer Rainless-day Frequencies for (a) Hudson Valley, (b) Ohio Valley, (c) Mississippi Valley, and (d) Southern Plains Regions.
Notes: Kernel density functions computed for four distinct periods of time: 1944–1978 (gray line), 1979–2013 (black line), 1994–2013 (blue line), and the full period (1944–2013; transparent red shading).

function for the Ohio Valley was flattened for the most recent 20 years relative to the full period (Figures S5–S7).

Spearman correlations between tree-ring reconstructions of summer PDSI and summer rainless-day frequencies were significantly negative in the Hudson Valley ($\rho = -0.66$), Ohio Valley ($\rho = -0.59$), Mississippi Valley ($\rho = -0.54$), and Southern Plains ($\rho = -0.46$) regions ($p < 0.001$ in all cases). For the extreme years of reconstructed PDSI, these correlations were also significantly negative, but stronger in all regions: Hudson Valley ($\rho = -0.74$), Ohio Valley ($\rho = -0.69$), Mississippi Valley ($\rho = -0.61$), and Southern Plains ($\rho = -0.52$) (Figure 7). Extremes in reconstructed PDSI were more strongly associated with rainless-day frequency across our study gradient. Spearman correlations between total summer precipitation and rainless days were significantly negative in the Hudson Valley ($\rho = -0.85$), Ohio Valley ($\rho = -0.72$), Mississippi Valley ($\rho = -0.66$), and Southern Plains ($\rho = -0.59$) (Figure S9).

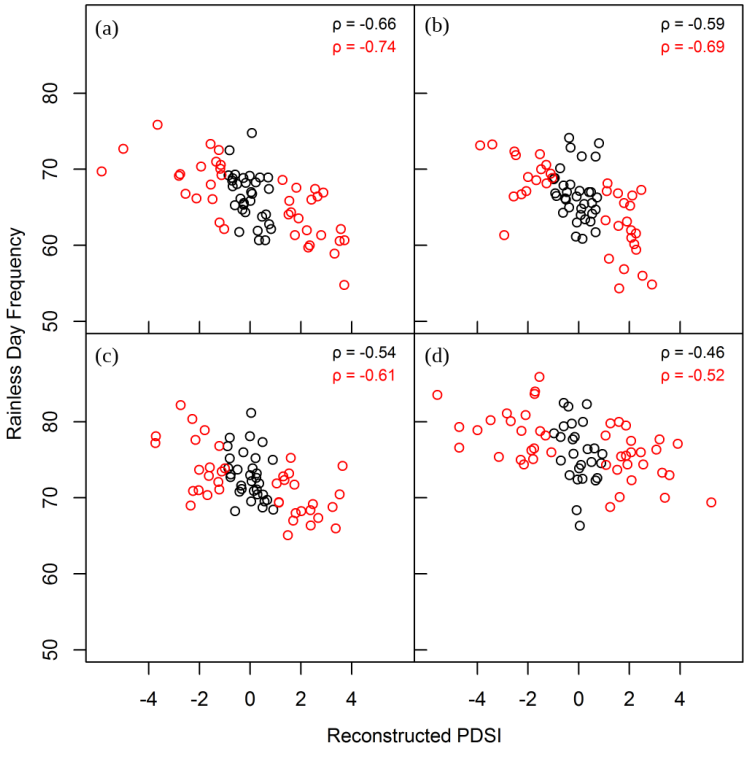

Figure 7. (Color online) Scatterplots of Reconstructed PDSI and Summer Rainless-day Frequency for (a) Hudson Valley, (b) Ohio Valley, (c) Mississippi Valley, and (d) Southern Plains Regions. *Notes*: Extreme years ($-1 >$ PDSI $> +1$) plotted in red. Spearman correlations for all years (black) and extreme years (red) displayed in upper right corners

3.4. *Reconstruction of hydroclimate in the Hudson Valley*

Tree-ring records from the Hudson Valley region helped us create a skillful model of total summer precipitation for 1525–2003 CE and summer rainless days for 1625–2001 CE (Figures 8 and S8). The common nest for the precipitation reconstruction accounted for 59.8% of the annual variance from 1957 to 1980 in the instrumental data (Figure S8 in the online supplemetary material), while the rainless-day reconstruction accounted for 46.3% of the annual variance (Figure 8); a year is lost at the end of both calibration models because of the prior-year lag in the tree-ring data. In the precipitation reconstruction, the first two principal components of the common nest are used for reconstruction for 1800–2001, 1750–1774, and 1500–1524, derived from a combination of 53 predictors from 32 chronologies; the remainder of the nests used only the first principal component. In contrast, the rainless-day reconstruction used only the first principal component of

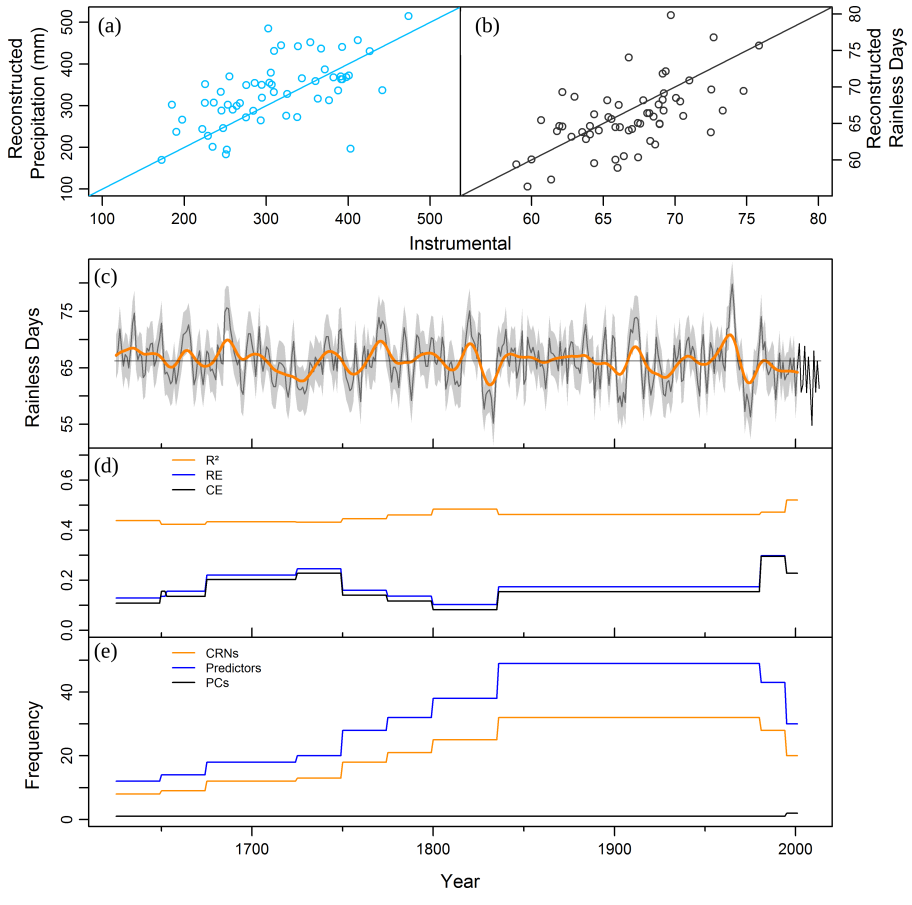

Figure 8. (Color online) Reconstructed Summer Hydroclimate in the Hudson Valley Region: Predicted versus Observed (Reconstructed versus Instrumental) Scatterplot (1944–2013) for Reconstructions of Total Summer (a) Precipitation and (b) Rainless days; (c) Rainless-day Reconstruction (dark gray) (1625–2001) with Instrumental Precipitation (black) (2002–2013), 20-year Smoothing Spline (orange) and Extrapolated Root Mean Square Error (RMSE; light gray shade); and Model Calibration Statistics (1625–2001): (d) Coefficient of Determination (R^2; orange), Reduction of Error (RE; blue), and Coefficient of Efficiency (CE; black), and (e) Sample Size of Predictors (Predict.; blue), Chronologies (CRNs; orange), and Principal Components (PCs; black) of Summer Rainless-day Frequency Reconstruction

the common nest, with the exception of the 2002 nest that used the first two principal components. The summer rainless days reconstruction used a combination of 49 predictors from 32 chronologies (Figures 8 and S8). Verification of both models passed all tests, the reduction of error and coefficient of efficiency statistics were all positive, and all subsequent backward nests accounted for $>40\%$ of the

annual variance. The reduction of error and coefficient of efficiency statistics became negative for the rainless days reconstruction with the 1600 CE nest. The precipitation reconstruction model never fails, but total tree replication across four chronologies falls below 12 trees before 1525 with most of those trees in one chronology. All forward nests account for greater than 40% variance and reduction of error and coefficient of efficiency statistics were positive until the 2004 nest for rainless days.

The reconstructions reflect the general pattern of the instrumental record. However, there is a tendency for the trees to overpredict during extreme events like the 1960s drought and the 1970s pluvial. Most seriously, they overpredict the number of rainless days by 10 days (reconstructed 79.8 days; instrumental observed 69.7 days) and underpredict the precipitation totals by 168.7 mm (reconstructed 50.8 mm; instrumental observed 219.5 mm) during the peak of the 1960s drought.

Through the use of forward nests, we have the possibility to test the strength and stability of the relationship between tree rings and total summer precipitation and rainless days over a longer period than the main calibration period of 1957–1980. These longer calibration periods were from 1957 to 1994 and 1957 to 2001. The amount of variance accounted for by the tree-ring records increased to 62.0% and 58.9% of the instrumental record of precipitation and for the instrumental record of rainless days to 55.2% and 48.4%, respectively, and all reduction of error and coefficient of efficiency statistics were positive (Figures 8 and S8). These findings indicate that the relation between tree-growth and summer precipitation and rainless days in the Hudson Valley is maintained despite the increase in available moisture after 1980 CE (Figure 2).

Because of the existing precipitation reconstruction in the Hudson Valley (Tipton *et al.* in review), we use the rainless days reconstruction to illustrate another potential aspect of the precipitation regime during extreme years. The long-term mean number of reconstructed Hudson Valley rainless days is 66.2, or 72% of the 92 days in summer. The fewest rainless days were reconstructed in 1833 (55.2, 60% of the summer). The most rainless days (79.8, 87% of summer) were reconstructed for 1965; again, the trees overpredict rainless days by 10 days compared to the instrumental data. In comparison, the mean number of rainless days during the last 10 years of instrumental data, 63.1 days, is 3.1 days below the long-term mean. Notable, uninterrupted stretches of elevated rainless days began in 1685 (7 years long), 1769 (8 years), 1816 (11 years), and 1907 (8 years). For comparison, all of these notable stretches equaled or exceeded the length of the only significant drought since 1944. The 1960's drought lasted 7 years and started in 1962. Extreme periods of decreased rainless

days include: 1652 (9 years) and two back-to-back events of 12 and 11 years starting in 1710 and 1724, respectively. In comparison, the 20th century had four similar periods of extreme rainless-day frequency, two 8-year events starting in 1918 and 1925 and the 9- and 7-year events starting in 1971 and 1984. Perhaps the most dynamic period in terms of rainfall frequency is found from 1807 to 1835 when two 9-year rainy periods bracket the dry 1816–1826 period (Figure 8).

4. Discussion

In evaluating changes in extreme moisture conditions in four regions in the eastern US, we identified five key findings. First, summer rainless-day frequency in the Hudson Valley and Ohio Valley regions has been decreasing during a period in which most of the extreme wet years have occurred. While it is well known that these two regions have experienced increases in total precipitation and a greater frequency of large, high-intensity rainfall events (IPCC 2014), we find that it is also raining more frequently during the summer. Second, the increase in more frequent rainfall coincides with the increase in extreme wet years since 1994. Third, in the Ohio Valley and Mississippi Valley, significant differences in the structure of precipitation events between extreme wet and extreme dry years during the growing-season occurred primarily in a narrow window between late May and late June, while other regions had no consistent differences in weekly structure of rainfall. Fourth, at the opposing end members of our transect we observed two distinct characterizations of extreme dry years relative to extreme wet years: (1) greater dry-spell frequency, but similar dry-spell duration in the Hudson Valley and (2) longer dry-spell duration, but similar dry-spell frequency in the Southern Plains. Fifth, extreme years of reconstructed summer PDSI were strongly correlated with total precipitation and rainless days. From these relations, paleoclimatic inference indicates the recent period of 1994–2013 might have been unusual compared to most other points over the last 500–1000 years.

Despite these recent increases in total summer precipitation and rainfall frequency, these regions are projected to experience increases in rainless-day frequency and warming-induced drying during the 21st century (Singh *et al.* 2013; Cook *et al.* 2014, 2015). Although there is no reason to expect that recent climate change will reflect future changes, we were unable to detect increasing rainless-day frequency during the summer in any of our study regions. If the eastern US shifts to that anticipated structure and frequency of rainfall, human, and natural systems will likely experience a substantial shock through disruption of ecological disturbance regimes and terrestrial productivity.

4.1. *Rainless-day frequencies — Temporal trends and implications for moisture availability*

Within the instrumental record, we observed that it has been raining more often on a daily basis during the summer over recent years in the Hudson and Ohio Valley regions. Our findings add to recent work indicating changes in extreme precipitation events through the intensification of severe rainfall events (Spierre and Wake 2010; Karl and Knight 1998). In contrast to more northerly regions, the Mississippi Valley and Southern Plains have experienced no significant changes in summer rainless-day frequency over recent years. Although the relationships between PDSI and rainless-day frequency are statistically significant, rainless days in the Mississippi Valley and Southern Plains appear to be less in phase with PDSI than the Hudson and Ohio Valley regions. In the Mississippi Valley, this disconnect is highlighted by a wet year in 1973, when ∼81% of the season was rainless (Figures 2 and 5(c)), indicating that in some circumstances soil moisture levels are not directly related to the number of days with rainfall.

Although the primary focus of this study was on summer, trends were detected in fall and winter in a few regions. Recent increases in fall rainless days in the Ohio Valley (Figure S6), concurrent with increases in fall precipitation (Table 1), seems to be following model projections suggesting less frequent, higher intensity precipitation events in the region (Singh *et al.* 2013). The Hudson and Mississippi Valley regions also experienced strong positive trends in fall precipitation, although the trends coincided with non-significant changes in fall rainless days. These trends may also be indicative of less frequent, higher intensity precipitation events in those regions during the fall. In addition, the flattening of the winter rainless-day frequency distribution for the most recent 20 years in the Ohio Valley indicates that recent winters in this region may have been more extreme in terms of higher interannual variability in the frequency of rainless (including snowless) days. Overall, increases in rainless-day frequency have yet to be broadly manifested across our gradient.

4.2. *Transient structure of wet and dry years*

While differences in the structure of growing-season precipitation were found between extreme wet and dry years in all regions, differences in weekly rainfall in the Ohio Valley and Mississippi Valley were restricted to the early portion of the growing season, mainly in May and June (Figure 3). Meanwhile, differences are largely insignificant and spread throughout the summer in the Hudson Valley and Southern Plains, indicating a more even, random temporal distribution of

disparities between extreme wet and dry years. This suggests that there is no temporal association for wet and dry years in the Hudson Valley and Southern Plains, and a probable dissociation between wet and dry years in the Ohio Valley and Mississippi Valley earlier in the summer months. Some caution is needed with these results as it is possible that they could also represent random differences between the two series. Nonetheless, prior work has shown a relationship between North American Monsoon patterns in the Southwest (high July–August precipitation) and high June precipitation in the south-central US (Higgins *et al.* 1997), but little has been evaluated beyond average regional anomalies. Further investigation into the possible synoptic-scale drivers of sub-seasonal precipitation trends could shed light on the causes. Incorporating a more spatially representative domain in both the southern United States and northern Mexico would help quantify the full North American Monsoon pattern.

Another subtle, but interesting, difference between extreme wet and dry years across our study gradient is related to dry-spell frequency and duration. The only significant differences between wet and dry years in the Hudson Valley were the increased frequency of dry spells, with minimal differences in duration of dry spells. In contrast, the only significant difference between wet and dry years moving south into the Southern Plains was found with the duration of dry spells, with minimal differences in the frequency of dry spells (Figure 4). These findings indicate that a sustained period of higher precipitation during wet years is the key to higher levels of total summer moisture especially in the center of our gradient, where both duration and frequency of dry spells were significant. If forecasts of extended lengths in dry spells are correct for the future, these changes might have the greatest impact on human and natural systems in regions within and near the northern end of our transect. An increase in dry-spell duration does not follow the general climatology of the past 70 years.

4.3. *Inferring rainfall structure during extreme years over the past millennium*

Using the strong relation between extreme reconstructed PDSI and rainless days, we can place recent patterns of rainless days into a long-term perspective (Figure 9). All regions in our transect appear to have a higher temporal clustering of extreme years over the 20th century, indicating that we may be observing high interannual variability in the number of rainless days compared to prior centuries. These inferences should be taken with caution as total precipitation is a stronger driver of tree growth. With the transient structure of rainfall in mind, wet years in the Hudson and Ohio Valley regions can likely be characterized by a decrease in

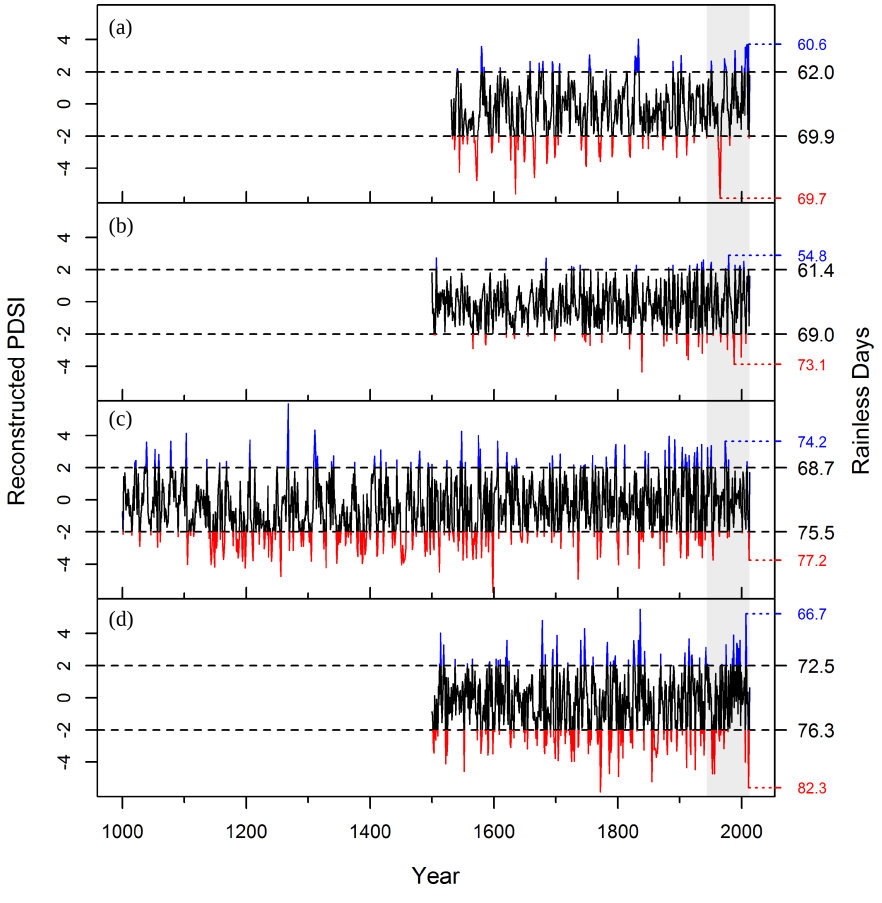

Figure 9. (Color online) PDSI Reconstructions with Extreme Dry (PDSI < -2; red) and Wet (PDSI $> +2$; blue) Years for (a) Hudson Valley, (b) Ohio Valley, (c) Mississippi Valley, and (d) Southern Plains Regions.

Notes: For each region, mean number of rainless days (1944–2013) for wet years (top dashed line) and dry years (bottom dashed line), number of rainless days for the wettest year (maximum PDSI; blue), and number of rainless days for the driest year (minimum PDSI; red) are on right *y*-axis. Shading represents 1944–2013.

dry-spell frequency while extremely dry years were likely characterized by more frequent dry spells.

In the Mississippi Valley and Southern plains, drought tends to be characterized by longer dry spells. This characterization is more strongly expressed in the Southern Plains where during the dry summer of 2011, there were 80.2 rainless days. The presence of the long-lived baldcypress (*Taxodium distichum* (L.) Rich.) in the Mississippi Valley allowed for the creation of a 1000-year reconstruction of moisture availability in the NADA (Table S2 in the online

supplementary material). Over that longer time frame, rainy summers were less common from 1100–1400 CE than the 20th century. We are not able to go as far back in time in the Southern Plains, but there was a higher frequency of dry summers during the 18th and 19th centuries and the latter portion of the 20th century in this region experienced one of the strongest pluvials of the last 500 years (Figure 9). In these two regions, the recent rainier periods likely had shorter dry spells compared to prior centuries. At this time, the recent uptick in drought and longer dry spells during the early portion of the 21st century appears to be a return to a more common long-term pattern, especially in the Southern Plains. Overall, paleoclimatic records suggest that summers during the latter half of the 20th century are less characteristic of the past few hundred years.

There are many reconstructions of hydroclimate in the eastern US (Cook and Krusic 2004; Cook *et al.* 2004; Stahle *et al.* 2007). We present the surprisingly strong rainless-day reconstruction in the Hudson Valley to enhance visualization of the structure of potential rainfall during extreme years over the past 400 years. The relation between tree rings and summer rainless days is driven by total summer precipitation in the Hudson Valley (Figure S8), but the strong relations between precipitation, rainless days, and the transient nature of precipitation during extreme years allows us to better infer summer hydroclimate. In the past, it is likely that extreme dry years were characterized by a higher frequency of dry spells and rainless days. It is possible that summers during the latter 1680s and early 1770s were characterized by small rainfall events interspersed with frequent dry spells and, perhaps, more sunlight. In contrast, 75.8% of the last 33 years had greater rainfall frequency than the 377-year mean. It appears only 1710–1735 CE matched the modern period in terms of potential rainless days and less-frequent dry spells. No years from 1710 to 1735 matched the extreme observed in 2011, although we take caution with this comparison given that 2011 is instrumental data. The opposing extremes between the 1960s drought and 1970s pluvial can only be compared to the late 1820s — early 1830s drought and late 1830s pluvial (Figure 8). It is clear that rainless days are strongly related to total precipitation. The preponderance of evidence in the instrumental and paleoclimatic records suggest the last four decades of hydroclimate in the Hudson Valley to be unusual compared to much of the period since 1625 CE.

4.4. *Ecological implications*

Moisture availability has been documented to be an important factor of tree growth across our study region (e.g., Cook 1991; Clark *et al.* forthcoming). The contributions of daily precipitation to the ecology of trees and forests at long time

scales are more of an open question as much work has been focused on seedlings or over short periods (e.g., Lewis and Tanner 2000; Hanson *et al.* 2001; Deslauriers *et al.* 2003; O'Brien *et al.* 2013). We add to these studies by finding that a network of trees over the Hudson Valley is sensitive to total summer precipitation and rainless days. A total of 10 of the 42 tree-ring chronologies in this network were collected for drought reconstructions. The remainder were targeted for their location near a northern range margin and an age >100 years (Pederson 2005). The age requirement could bias trees toward less productive or drier sites where older trees are more often found (Stahle and Chaney 1994). Despite these potential biases, that the number of rainless days accounts for nearly one-half of the average annual stem growth was not expected. With the hindsight that dry years exhibit more frequent dry spells than wet years in the Hudson Valley and that trees in the northeastern US are more sensitive to precipitation than similar trees in the southeastern US (Martin-Benito and Pederson 2015), these findings are reasonable. Recent work further establishes that moisture availability in the eastern US matters to trees from a range of genera and site types (e.g., Pederson *et al.* 2012; Brzostek *et al.* 2014; Clark *et al.* 2014). In fact, research in the Southern Appalachian Mountains indicates that a decline in the number of small storms and increased time between rainfall events will result in growth reductions (Elliott *et al.* 2015). Continued documentation of the impacts of frequency, temporal clustering, and intensity of rainfall events on forest productivity would inform forest management and conservation efforts.

The impacts of changing rainless-day frequency and other extreme hydroclimatic events on disturbance and forest dynamics will be complex. There are likely nonlinear and threshold relationships between transient climate during and after these events that need consideration (Cavin *et al.* 2013). Drought can be an important factor of canopy tree mortality in the eastern US (e.g., Clinton *et al.* 1993; Olano and Palmer 2003). An increase in dry-spell frequency or duration would likely increase the stress of canopy trees and increase their vulnerability to decline and increased mortality rates (Pedersen 1998; Bendixsen *et al.* 2015). Changes in transient precipitation could also impact the frequency or size of wildfire. From 2001–2008, where 99.9% of the recorded fires were classified as anthropogenic, up to 32% of the variance in area burned and number of fires was accounted for by precipitation; reduced rainfall led to more frequent and larger fires in a region adjacent to our Ohio Valley region (Lynch and Hessl 2010). Across 34 national forests and parks approximately 800 km east of our Ohio Valley study region, daily precipitation variability from 1971 to 2000 accounted for fire more strongly than annual precipitation (Lafon and Quiring 2012). These examples are but a few of the many potential feedbacks of transient precipitation on ecological processes.

More research is needed to understand the complex interactions between the distribution of daily rainfall and forest ecology.

Acknowledgments

Partial support for this research comes from the National Science Foundation EF-1241930, which supports the PalEON Project (paleonproject.org), and from the Harvard Forest. We thank A. P. Williams, D. Singh, M. Lau, E. Cook, and B. Cook for feedback that improved data analysis. We thank A. P. Williams, D. Foster, M. Duveneck, D. Orwig, and A. Barker-Plotkin, and two anonymous reviewers whose comments improved the manuscript.

References

Allen, CD, Macalady AK, Chenchouni H, Bachelet D *et al.* (2010). A global overview of drought and heat-induced tree mortality reveals emerging climate change risks for forests. *Forest Ecology and Management*, 259(4): 660–684.

Auclair, AN (1993). Extreme climatic fluctuations as a cause of forest dieback in the Pacific Rim. *Water, Air, and Soil Pollution*, 66(3–4): 207–229.

Bartlein, PJ, Harrison SP, Brewer S, Connor S *et al.* (2011). Pollen-based continental climate reconstructions at 6 and 21 ka: A global synthesis. *Climate Dynamics*, 37(3–4): 775–802.

Bendixsen, DP, Hallgren SW and Frazier AE (2015). Stress factors associated with forest decline in xeric oak forests of south-central United States. *Forest Ecology and Management*, 347: 40–48.

Brunetti, M, Maugeri M and Nanni T (2001). Changes in total precipitation, rainy days and extreme events in northeastern Italy. *International Journal of Climatology*, 21(7): 861–871.

Brzostek, ER, Dragoni D, Schmid HP, Rahman AF *et al.* (2014). Chronic water stress reduces tree growth and the carbon sink of deciduous hardwood forests. *Global Change Biology*, 20(8): 2531–2539.

Carbone, MS, Czimczik CI, Keenan TF, Murakami PF, Pederson N *et al.* (2013). Age, allocation, and availability of nonstructural carbon in mature red maple trees. *New Phytologist*, 200: 1145–1155.

Cavin, L, Mountford EP, Peterken GF and Jump AS (2013). Extreme drought alters competitive dominance within and between tree species in a mixed forest stand. *Functional Ecology*, 27(6): 1424–1435.

Clark, JS, Iverson L, Woodall CW, Allen CD *et al.* (forthcoming). The impacts of increasing drought on forest dynamics, structure, diversity, and management. *Global Change Biology.*

Clark, JS, Bell DM, Kwit MC and Zhu K (2014). Competition-interaction landscapes for the joint response of forests to climate change. *Global Change Biology*, 20(6): 1979–1991.

Cleaveland, MK, Votteler TH, Stahle DK, Casteel RC and Banner JL (2011). Extended chronology of drought in south central, southeastern and west Texas. *Texas Water Journal*, 2(1): 54–96.

Clinton, BD, Boring LR and Swank WT (1993). Canopy gap characteristics and drought influences in oak forests of the Coweeta Basin. *Ecology*, 74: 1551–1558.

Cook, BI, Ault TR and Smerdon JE (2015). Unprecedented 21st century drought risk in the American Southwest and Central Plains. *Science Advances*, 1(1): e1400082.

Cook, BI, Smerdon JE, Seager R and Coats S (2014). Global warming and 21st century drying. *Climate Dynamics*, 43(9–10): 2607–2627.

Cook, ER (1991). Tree rings as indicators of climatic change and the potential response of forests to the greenhouse effect. In: R Wyman (ed.) *Global Climate Change and Life on Earth*, London, Routledge: Chapman & Hall, pp. 56–64.

Cook, ER and Kairiukstis LA (eds.) (1990). *Methods of Dendrochronology: Applications in the Environmental Sciences*. Dordrecht, Netherlands: Kluwer Academic Publishers.

Cook, ER and Krusic PJ (2004). North American summer PDSI reconstructions. IGBP PAGES/World Data Center for Paleoclimatology Data Contribution Series, 45.

Cook, ER, Krusic PJ and Jones PD (2003). Dendroclimatic signals in long tree-ring chronologies from the Himalayas of Nepal. *International Journal of Climatology*, 23: 707–732.

Cook, ER and Peters K (1981). The smoothing spline: A new approach to standardizing forest interior tree-ring width series for dendroclimatic studies. *Tree-Ring Bulletin*.

Cook, ER, Bartlein PJ, Diffenbaugh N, Seager R *et al.* (2008). Hydrological variability and change. *Abrupt Climate Change*, 143–257.

Cook, ER, Briffa KR, Meko DM, Graybill DA and Funkhouser G (1995). The 'segment length curse' in long tree-ring chronology development for palaeoclimatic studies. *The Holocene*, 5(2): 229–237.

Cook, ER, Meko DM, Stahle DW and Cleaveland MK (1996). Tree-ring reconstructions of past drought across the coterminous United States: Tests of a regression method and calibration/verification results. In: *Tree Rings, Environment, and Humanity*. Tucson: Radiocarbon, pp. 155–169.

Cook, ER, Meko DM, Stahle DW and Cleaveland MK (1999). Drought reconstructions for the continental United States. *Journal of Climate*, 12(4): 1145–1162.

Cook, ER, Seager R, Cane MA and Stahle DW (2007). North American drought: Reconstructions, causes, and consequences. *Earth-Science Reviews*, 81(1): 93–134.

Cook, ER, Woodhouse CA, Eakin CM, Meko DM and Stahle DW (2004). Long-term aridity changes in the western United States. *Science*, 306(5698): 1015–1018.

DeGaetano, AT (2009). Time-dependent changes in extreme-precipitation return-period amounts in the continental United States. *Journal of Applied Meteorology and Climatology*, 48(10): 2086–2099.

Deslauriers, A, Morin H, Urbinati C and Carrer M (2003). Daily weather response of balsam fir (Abies balsamea (L.) Mill.) stem radius increment from dendrometer analysis in the boreal forests of Québec (Canada). *Trees*, 17(6): 477–484.

Douglass, AE (1919). *Climatic Cycles and Tree-Growth*. Vol. 1. Washington: Carnegie Institution of Washington.

Easterling, DR, Meehl GA, Pamesan C, Changnon SA, Karl TR and Mearns L (2000). Climate extremes: Observations, modelling, and impacts. *Science*, 289(5487): 2068–2074.

Elliott, KJ, Miniat CF, Pederson N and Laseter SH (2015). Forest tree growth response to hydroclimate variability in the southern Appalachians. *Global Change Biology*, doi: 10.1111/gcb.13045.

Fritts, HC (1976). *Tree Rings and Climate*. San Diego, CA: Academic Press.

Fritts, HC (1991). *Reconstructing Large-scale Climatic Patterns from Tree-ring Data*. Tuscan, AZ: University of Arizona Press.

Giorgi, F, Im ES, Coppola E, Diffenbaugh NS *et al.* (2011). Higher hydroclimatic intensity with global warming. *Journal of Climate*, 24(20): 5309–5324.

Hanson, PJ, Todd DE and Amthor JS (2001). A six-year study of sapling and large-tree growth and mortality responses to natural and induced variability in precipitation and throughfall. *Tree Physiology*, 21(6): 345–358.

Higgins, RW, Yao Y and Wang XL (1997). Influence of the North American monsoon system on the US summer precipitation regime. *Journal of Climate*, 10(10): 2600–2622.

Holmes, RL (1983). Computer-assisted quality control in tree-ring dating and measurement. *Tree-Ring Bulletin*, 43(1): 69–78.

Holst, J, Barnard R, Brandes E, Buchmann N, Gessler A and Jaeger L (2008). Impacts of summer water limitation on the carbon balance of a Scots pine forest in the southern upper Rhine plain. *Agricultural and Forest Meteorology*, 148(11): 1815–1826.

Hubeny, JB, King JW and Reddin M (2011). Northeast US precipitation variability and North American climate teleconnections interpreted from late Holocene varved sediments. *Proceedings of the National Academy of Sciences*, 108(44): 17895–17900.

IPCC (2014). *Climate Change 2014: Impacts, Adaptation, and Vulnerability. Part B: Regional Aspects*. Contribution of Working Group II to the Fifth Assessment Report of the Intergovernmental Panel on Climate Change. Barros, VR, CB Field, DJ Dokken, MD Mastrandrea *et al.* (eds.). Cambridge, United Kingdom and New York, NY: Cambridge University Press.

Jacoby, GC Jr. and D'Arrigo R (1989). Reconstructed Northern Hemisphere annual temperature since 1671 based on high-latitude tree-ring data from North America. *Climatic Change*, 14(1): 39–59.

Kagawa, A, Sugimoto A and Maximov TC (2006). $^{13}CO_2$ pulse labelling of photoassimilates reveals carbon allocation within and between tree rings. *Plant, Cell and Environment*, 29: 1571–1584.

Karl, TR and Easterling DR (1999). Climate extremes: Selected review and future research directions. In *Weather and Climate Extremes*. Netherlands: Springer, pp. 309–325.

Karl, TR and Knight RW (1998). Secular trends of precipitation amount, frequency, and intensity in the United States. *Bulletin of the American Meteorological Society*, 79(2): 231–241.

Kruskal, WH and Wallis WA (1952). Use of ranks in one-criterion variance analysis. *Journal of the American Statistical Association*, 47(260): 583–621.

Kunkel, KE (2003). North American trends in extreme precipitation. *Natural Hazards*, 29(2): 291–305.

Kunkel, KE, Easterling DR, Redmond K and Hubbard K (2003). Temporal variations of extreme precipitation events in the United States: 1895–2000. *Geophysical Research Letters*, 30(17).

Lafon, CW and Quiring SM (2012). Relationships of fire and precipitation regimes in temperate forests of the eastern United States. *Earth Interactions*, 16: 1–15.

Lewis, SL and Tanner EV (2000). Effects of above-and belowground competition on growth and survival of rain forest tree seedlings. *Ecology*, 81(9): 2525–2538.

Lucero, OA and Rozas D (2002). Characteristics of aggregation of daily rainfall in a middle-latitudes region during a climate variability in annual rainfall amount. *Atmospheric Research*, 61(1): 35–48.

Lynch, C and Hessl A (2010). Climatic controls on historical wildfires in West Virginia, 1939–2008. *Physical Geography*, 31: 254–269.

Mallakpour, I and Villarini G (2015). The changing nature of flooding across the central United States. *Nature Climate Change*, 5(3): 250–254.

Martin-Benito, D and Pederson N (2015). Convergence in drought stress, but a divergence of climatic drivers across a latitudinal gradient in a temperate broadleaf forest. *Journal of Biogeography*, doi: 10.1111/jbi.12462.

Massey, FJ Jr. (1951). The Kolmogorov-Smirnov test for goodness of fit. *Journal of the American Statistical Association*, 46(253): 68–78.

Matonse, AH and Frei A (2013). A seasonal shift in the frequency of extreme hydrological events in southern New York State. *Journal of Climate*, 26(23): 9577–9593.

Meko, D (1997). Dendroclimatic reconstruction with time varying predictor subsets of tree indices. *Journal of Climate*, 10(4): 687–696.

Melillo, JM, Richmond T and Yohe GW (eds.) (2014). Climate Change Impacts in the United States: The Third National Climate Assessment, U.S. Global Change Research Program, doi: 10.7930/J0Z31WJ2.

Newby, PE, Shuman BN, Donnelly JP, Karnauskas KB and Marsicek J (2014). Centennial-to-millennial hydrologic trends and variability along the North Atlantic Coast, USA, during the Holocene. *Geophysical Research Letters*, 41(12): 4300–4307.

O'Brien, MJ, Philipson CD, Tay J and Hector A (2013). The influence of variable rainfall frequency on germination and early growth of shade-tolerant dipterocarp seedlings in Borneo. *PloS One*, 8(7): e70287.

Olano, JM and Palmer MW (2003). Stand dynamics of an Appalachian old-growth forest during a severe drought episode. *Forest Ecology and Management*, 174(1): 139–148.

Pedersen, BS (1998). The role of stress in the mortality of midwestern oaks as indicated by growth prior to death. *Ecology*, 79(1): 79–93.

Pederson, N (2005). Climatic sensitivity and growth of southern temperate trees in the eastern US: Implications for the carbon cycle, PhD Dissertation, Columbia University.

Pederson, N, Bell AR, Cook ER *et al.* (2013). Is an epic pluvial masking the water insecurity of the greater New York City region? *Journal of Climate*, 26(4): 1339–1354.

Pederson, N, Cook ER, Jacoby GC, Peteet DM and Griffin KL (2004). The influence of winter temperatures on the annual radial growth of six northern-range-margin tree species. *Dendrochronologia*, 22: 7–29.

Pederson, N, Tackett K, McEwan RW, Clark S *et al.* (2012). Long-term drought sensitivity of trees in second-growth forests in a humid region. *Canadian Journal of Forest Research*, 42(10): 1837–1850.

Peterson, TC, Zhang X, Brunet-India M and Vázquez-Aguirre JL (2008). Changes in North American extremes derived from daily weather data. *Journal of Geophysical Research: Atmospheres (1984–2012)*, 113(D7).

Plaut, JA, Wadsworth WD, Pangle R, Yepez EA, McDowell NG and Pockman WT (2013). Reduced transpiration response to precipitation pulses precedes mortality in a pinon–juniper woodland subject to prolonged drought. *New Phytologist*, 200(2): 375–387.

Polade, SD, Pierce DW, Cayan DR, Gershunov A and Dettinger MD (2014). The key role of dry days in changing regional climate and precipitation regimes. *Scientific Reports*, 4: 4364.

R Development Core Team (2012). R: A language and environment for statistical computing. Vienna, Austria: R Foundation for Statistical Computing.

Seager, R, Pederson N, Kushnir Y, Nakamura J and Jurburg S (2012). The 1960s drought and the subsequent shift to a wetter climate in the Catskill Mountains region of the New York City watershed. *Journal of Climate*, 25(19): 6721–6742.

Sen, PK (1968). Estimates of the regression coefficient based on Kendall's tau. *Journal of the American Statistical Association*, 63(324): 1379–1389.

Singh, D, Tsiang M, Rajaratnam B and Diffenbaugh NS (2013). Precipitation extremes over the continental United States in a transient, high-resolution, ensemble climate model experiment. *Journal of Geophysical Research: Atmospheres*, 118(13): 7063–7086.

Spearman, C (1904). The proof and measurement of association between two things. *The American Journal of Psychology*, 15(1): 72–101.

Spierre, SG and Wake C (2010). Trends in Extreme Precipitation Events for the Northeastern United States 1948–2007, Carbon Solutions New England Report and Clean Air-Cool Planet Report.

St. George, S and Ault TR (2014). The imprint of climate within Northern Hemisphere trees. *Quaternary Science Reviews*, 89: 1–4.

Stahle, DW and Chaney PL (1994). A predictive model for the location of ancient forests. *Natural Areas Journal*, 14(3): 151–158.

Stahle, DW, Fye FK, Cook ER and Griffin RD (2007). Tree-ring reconstructed megadroughts over North America since AD 1300. *Climatic Change*, 83(1–2): 133–149.

Stokes, MA and Smiley TL (1968). *Tree-ring Dating*. University of Chicago Press.

Thibeault, JM and Seth A (2014). Changing climate extremes in the Northeast United States: Observations and projections from CMIP5. *Climatic Change*, 127(2): 273–287.

Tipton, J, Hooten M, Pederson N, Tingley M and Bishop DA (2015). Reconstruction of late Holocene climate based on tree growth and mechanistic hierarchical models. *Environmetrics*, DOI: 10.1002/env.2368.

Trumbore, S, Gaudinski J, Hanson P and Southon J (2002). Quantifying ecosystem-atmosphere carbon exchange with a ^{14}C label. Eos, Trans. *American Geophysical Union*, 83(24): 265–268.

Viau, AE, Gajewski K, Sawada MC and Fines P (2006). Millennial-scale temperature variations in North America during the Holocene. *Journal of Geophysical Research: Atmospheres (1984–2012)*, 111(D9).

Villarini, G, Smith JA and Veechi GA (2013). Changing frequency of heavy rainfall over the central United States. *Journal of Climate*, 26: 351–357.

Vose, RS, Applequist S, Squires M, Durre I, *et al.* (2014). Improved historical temperature and precipitation time series for US climate divisions. *Journal of Applied Meteorology and Climatology*, 53(5): 1231–1251.

Weider, K and Boutt DF (2010). Heterogeneous water table response to climate revealed by 60 years of ground water data. *Geophysical Research Letters*, 37(24).

West, JB, Bowen GJ, Cerling TE and Ehleringer JR (2006). Stable isotopes as one of nature's ecological recorders. *Trends in Ecology & Evolution*, 21(7): 408–414.

Williams, CN, Vose RS, Easterling DR and Menne MJ (2006). United States historical climatology network daily temperature, precipitation, and snow data. ORNL/CDIAC-118, NDP-070. Carbon Dioxide Information Analysis Center, Oak Ridge National Laboratory, US Department of Energy, Oak Ridge, Tennessee.

Williams, AP, Michaelsen J, Leavitt SW and Still CJ (2010). Using tree rings to predict the response of tree growth to climate change in the continental United States during the twenty-first century. *Earth Interactions*, 14(19): 1–20.

Supplemental Material

Table S1. Summary of Instrumental Records (US Historical Climatology Network) used for Hudson Valley (HV), Ohio Valley (OV), Mississippi Valley (MV), and Southern Plains (SP) (1944–2013)

						Mean Total Precipitation				Number of Years Meeting Criteria			
Station ID	Latitude	Longitude	Elevation	State	Region	Spring	Summer	Fall	Winter	Spring	Summer	Fall	Winter
USH00031632	36.42	−90.59	91.4	AR	MV	371.0	263.3	287.7	289.9	67	68	68	66
USH00034572	36.49	−91.54	153.0	AR	MV	337.2	253.7	288.5	263.3	63	62	64	60
USH00035186	35.60	−91.27	69.5	AR	MV	381.4	271.4	305.1	306.1	67	68	69	69
USH00035820	36.26	−90.97	96.0	AR	MV	366.9	258.8	303.0	301.2	67	65	70	66
USH00110187	37.48	−89.23	195.1	IL	MV	387.0	287.8	279.0	280.4	68	68	69	69
USH00231364	36.17	−89.66	82.3	MO	MV	370.8	270.9	281.8	310.2	62	65	64	62
USH00232289	36.62	−90.81	88.1	MO	MV	373.4	277.7	298.7	277.4	69	70	68	67
USH00235253	37.30	−89.97	118.9	MO	MV	373.9	302.2	287.7	255.7	66	70	69	69
USH00235834	37.15	−92.26	442.0	MO	MV	328.9	285.4	281.3	199.7	67	66	68	69
USH00402108	35.55	−89.70	117.3	TN	MV	406.1	275.1	306.5	364.8	70	69	69	70
USH00409219	36.39	−89.03	106.7	TN	MV	380.9	293.1	299.2	335.9	70	70	69	68
USH00150254	38.45	−82.61	170.7	KY	OV	288.6	303.2	220.1	242.1	67	66	64	60
USH00152791	38.12	−83.55	207.3	KY	OV	328.1	337.1	242.5	262.3	70	70	70	69
USH00336781	38.76	−82.89	164.6	OH	OV	301.5	298.8	210.3	229.1	70	69	70	69
USH00338830	39.11	−82.98	170.7	OH	OV	290.8	291.8	205.2	214.1	64	64	66	53
USH00467029	37.57	−81.54	390.1	WV	OV	315.0	334.7	236.2	255.3	63	62	64	61
USH00468384	38.80	−81.36	287.4	WV	OV	294.0	325.1	248.4	242.0	66	68	69	67
USH00469683	38.53	−81.92	186.2	WV	OV	278.9	293.8	222.4	221.2	67	70	68	66
USH00062658	41.95	−73.37	167.6	CT	HV	271.3	326.7	291.2	224.3	70	67	69	67
USH00190120	42.39	−72.54	45.7	MA	HV	276.7	301.2	287.3	237.8	69	70	68	68
USH00280907	40.90	−74.40	85.3	NJ	HV	314.5	329.8	309.5	250.3	61	61	60	57
USH00281582	41.03	−74.42	231.6	NJ	HV	334.6	343.1	331.1	281.3	66	64	65	66

Table S1. (*Continued*)

						Mean Total Precipitation				Number of Years Meeting Criteria			
Station ID	Latitude	Longitude	Elevation	State	Region	Spring	Summer	Fall	Winter	Spring	Summer	Fall	Winter
USH00283029	40.56	−74.88	79.2	NJ	HV	317.5	344.2	291.5	270.2	68	65	66	67
USH00300042	42.74	−73.81	83.8	NY	HV	237.1	273.4	239.4	186.3	70	70	70	70
USH00301752	42.72	−74.93	383.1	NY	HV	266.4	311.2	270.8	204.0	69	67	70	64
USH00302129	41.01	−73.83	61.0	NY	HV	333.6	324.1	324.0	290.6	64	62	64	67
USH00305426	41.77	−74.16	379.5	NY	HV	324.1	331.3	318.7	272.4	70	68	70	70
USH00305801	40.78	−73.97	39.6	NY	HV	307.2	315.1	294.6	258.4	70	70	70	70
USH00309292	41.39	−73.96	97.5	NY	HV	312.6	327.3	331.8	274.5	67	69	70	68
USH00360106	40.65	−75.45	118.9	PA	HV	281.8	327.0	282.4	239.0	70	70	70	70
USH00367029	41.74	−75.45	548.6	PA	HV	305.1	339.1	322.5	245.5	68	63	68	67
USH00431243	43.38	−72.60	256.6	VT	HV	285.6	299.7	291.2	245.3	69	70	69	70
USH00340179	34.59	−99.33	420.6	OK	SP	197.9	211.8	170.4	77.9	66	67	61	66
USH00340292	34.17	−97.13	268.2	OK	SP	280.0	225.9	239.4	146.7	67	64	64	66
USH00342944	35.22	−99.86	627.9	OK	SP	200.3	208.5	157.6	66.3	67	65	67	68
USH00343821	35.82	−97.40	338.3	OK	SP	270.7	266.0	223.8	107.9	66	67	69	65
USH00344204	34.99	−99.05	474.3	OK	SP	206.0	202.3	164.9	67.2	67	67	66	65
USH00344861	35.86	−97.93	320.0	OK	SP	249.9	259.1	196.6	95.7	69	68	68	65
USH00345063	34.61	−98.46	350.5	OK	SP	249.2	227.0	197.4	103.0	64	61	60	62
USH00345509	34.89	−99.50	486.2	OK	SP	196.8	206.1	166.6	69.1	68	65	63	68
USH00346926	34.73	−97.28	286.5	OK	SP	296.2	238.6	245.9	141.9	65	66	63	64
USH00349422	35.52	−98.70	493.2	OK	SP	215.9	242.3	180.3	79.3	67	66	63	65

Table S2. Chronologies used and their Statistics for the Hudson Valley Rainless Days and Precipitation Reconstructions

Site	Species	Chronology Span	Number of Series	EPS	Med. Seg. (yrs)	Comments (source)
Albany-Middleburgh, NY	QUlue	1507–2002	63	0.944	168	Live trees = *Quercus montana*; dead trees = *Q*. subgenus *Leucobalanus* species from Albany, NY region; (Pederson *et al.* 2013)
Bigelow, CT	TSCA	1643–1985	31	0.974	241	(International Tree Ring Databank (ITRDB))
Dingmans Falls, PA	TSCA	1609–1981	29	0.965	244	(ITRDB)
Greenbrook Sanctuary, NJ	CAGL	1818–2000	18	0.883	105	(Pederson *et al.* 2013)
Greenbrook Sanctuary, NJ	LITU	1750–2000	27	0.918	152	(Pederson *et al.* 2013)
Goose Egg Forest, NY	QUAL	1666–2002	35	0.963	186	(Pederson *et al.* 2013)
Goose Egg Forest, NY	QUMO	1666–2002	31	0.958	163	(Pederson *et al.* 2013)
Goose Egg Forest, NY	QURU	1799–2001	34	0.968	178	(Pederson *et al.* 2013)
Hunter Island, Bronx, NY	QUST	1773–2002	26	0.901	196	Trees date to British occupation during the Revolutionary War; (Pederson *et al.* 2013)
Hutchinson Forest, NJ	QU spp.	1563–1982	70	0.964	187	Living *trees* = *Q. alba*; dead trees = *Q*. subgenus *Leucobalanus* species from New Brunswick, NJ area; (ITRDB; Pederson *et al.* 2013)
Lake George, NY	QUVE	1836–2002	32	0.972	135	(Pederson *et al.* 2013)
Lincoln Mountain, NY	NYSY	1437–2000	54	0.966	355	(Pederson 2005)
Lisha Kill, NY	CAGL	1753–2002	27	0.914	150	(Pederson *et al.* 2013)
Lisha Kill, NY	QUAL	1816–2002	23	0.935	157	(Pederson *et al.* 2013)
Middleburgh, NY	JUVI	1449–2004	26	0.860	152	Live & dead wood; (Pederson *et al.* 2013)
Mohegan Plains, MA	PIRI	1802–1992	42	0.959	80	(ITRDB)

Table S2. (*Continued*)

Site	Species	Chronology Span	Number of Series	EPS	Med. Seg. (yrs)	Comments (source)
Mohonk, NY	BELE	1614–2002	29	0.950	129	Collected in 1974 & 2002; (ITRDB; Pederson *et al.* 2013)
Mohonk, NY	CAGL	1740–2002	30	0.940	152	(Pederson *et al.* 2013)
Mohonk, NY	PIRI	1618–1996	45	0.967	210	Approximate location; (Cook *et al.* 1999; ITRDB)
Mohonk, NY	QUlue	1449–2002	157	0.981	158	Living portion is *Q. montana*; the historical timbers portion is *Q.* subgenus *Leucobalanus* species from timbers in the New Paltz, NY area; (ITRDB; Pederson *et al.* 2013)
Mohonk, NY	QUVE	1793–2002	27	0.959	162	(Pederson *et al.* 2013)
Mohonk, NY	TSCA	1626–2002	43	0.973	243	Humpty Dumpty talus; (ITRDB; Pederson *et al.* 2013)
Mohonk, NY	TSCA	1658–2004	39	0.963	211	Rock Rift R; (ITRDB; Pederson *et al.* 2013)
Montgomery Place, NY	LITU	1754–2002	20	0.905	113	(Pederson *et al.* 2013)
Montgomery Place, NY	QUMO	1727–2002	33	0.941	179	(Pederson *et al.* 2013)
Montgomery Place, NY	QURU	1787–2002	28	0.928	130	(Pederson *et al.* 2013)
North Forty, CT	TSCA	1650–1985	32	0.970	196	(ITRDB)
Pack Forest, NY	TSCA	1453–2003	89	0.970	208	Orig. Pack For. TSCA, western MA update & historical timbers; (ITRDB; Pederson *et al.* 2013)
Palmaghatt, NY	BEAL	1730–2013	34	0.868	128	(ITRDB)
Palmaghatt, NY	QUMO	1777–2011	25	0.846	131	(ITRDB)
Prospect Mountain, NY	BELE	1820–2001	24	0.915	121	(Pederson *et al.* 2013)
Prospect Mountain, NY	CAOV	1775–2001	29	0.939	165	(Pederson *et al.* 2013)
Prospect Mountain, NY	QUAL	1659–2001	32	0.966	191	(Pederson *et al.* 2013)

Table S2. (*Continued*)

Site	Species	Chronology Span	Number of Series	EPS	Med. Seg. (yrs)	Comments (source)
Prospect Mountain, NY	QURU	1816–2001	28	0.934	127	(Pederson *et al.* 2013)
Ricketts Glen, PA	TSCA	1637–1981	26	0.947	242	(ITRDB)
Salt Springs, PA	TSCA	1619–1981	34	0.974	283	(ITRDB)
Schenectady, NY	QUVE	1802–2001	24	0.927	167	(Pederson *et al.* 2013)
Schunnemunk Mtn, NY	QUAL	1648–2001	46	0.928	244	Collected in 1983 & 2001; (ITRDB; Pederson *et al.* 2013)
Uttertown, NJ	LITU	1732–2003	28	0.961	147	(Pederson *et al.* 2013)
Uttertown, NJ	QUspp	1491–2002	65	0.956	206	Live trees = *Q montana*; historical timbers = *Q*. subgenus *Leucobalanus* species from northeastern NJ area; (Pederson *et al.* 2013)
Uttertown, NJ	QURU	1785–2001	44	0.979	131	(Pederson *et al.* 2013)

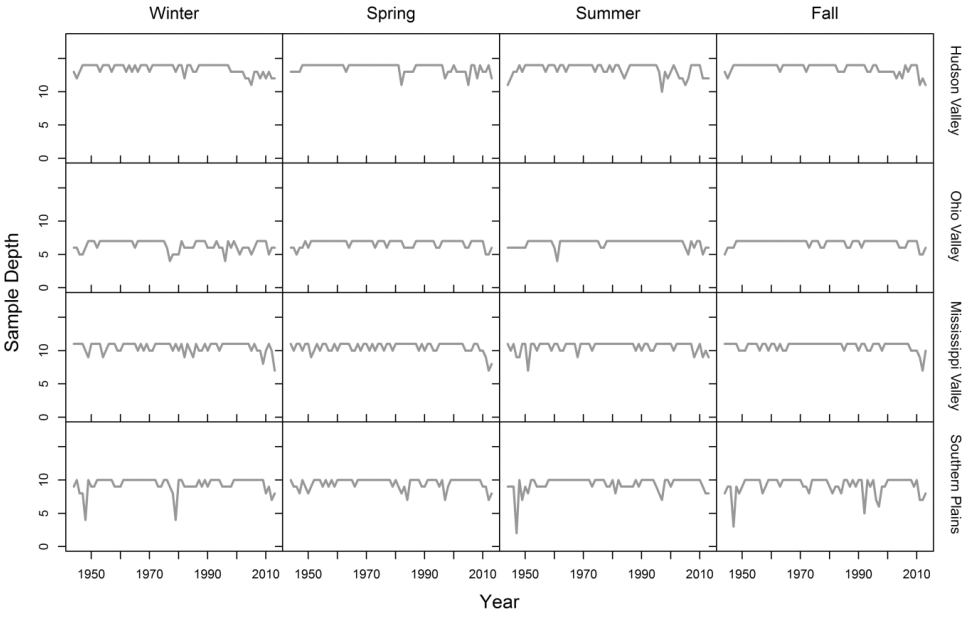

Figure S1. Instrumental Records Sample Depth (Number of Stations) by Year for Each Region and Season

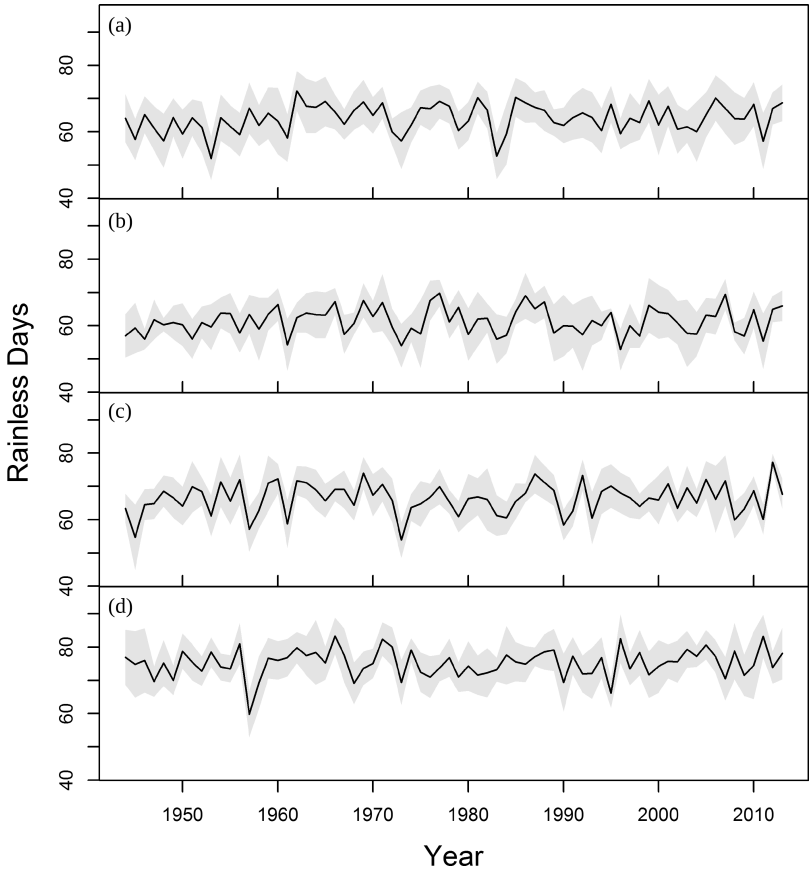

Figure S2. Mean **Spring** Rainless-day Frequencies (< 1 mm; Black Lines) for (a) Hudson Valley, (b) Ohio Valley, (c) Mississippi Valley, and (d) Southern Plains Regions with 95% Confidence Interval (gray shading) (1944–2013)

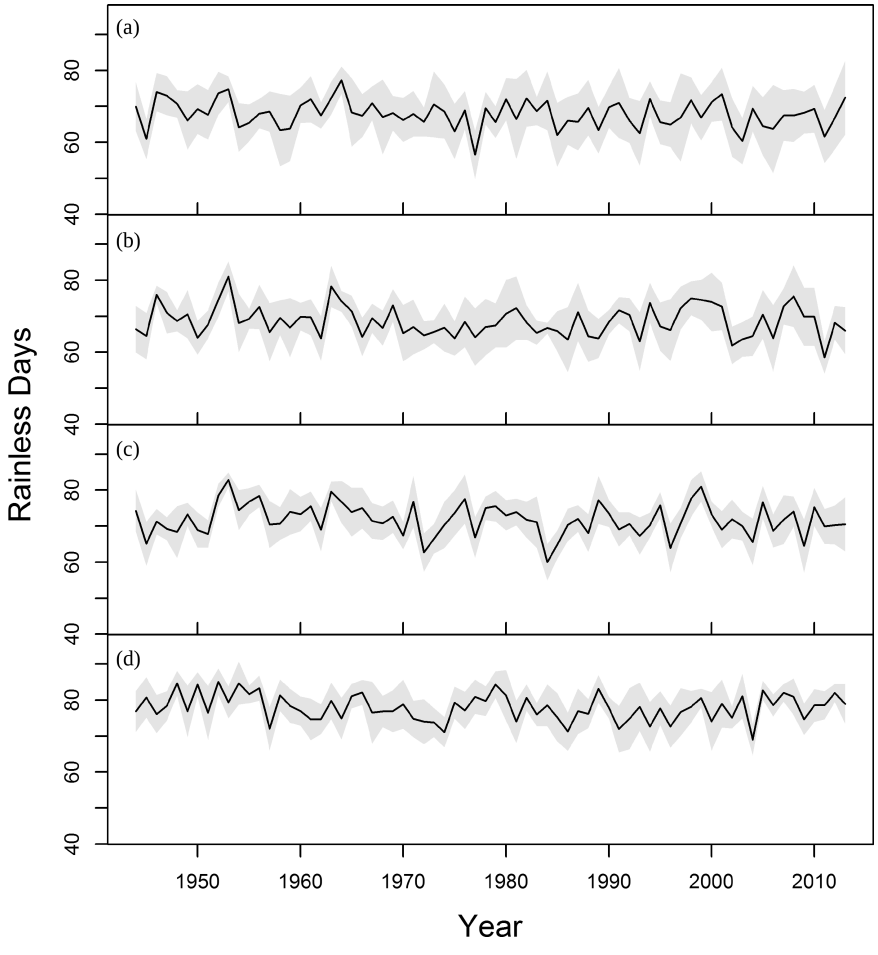

Figure S3. Mean **Fall** Rainless-day Frequencies (< 1 mm; Black Lines) for (a) Hudson Valley, (b) Ohio Valley, (c) Mississippi Valley, and (d) Southern Plains Regions with 95% Confidence Interval (gray shading) (1944–2013)

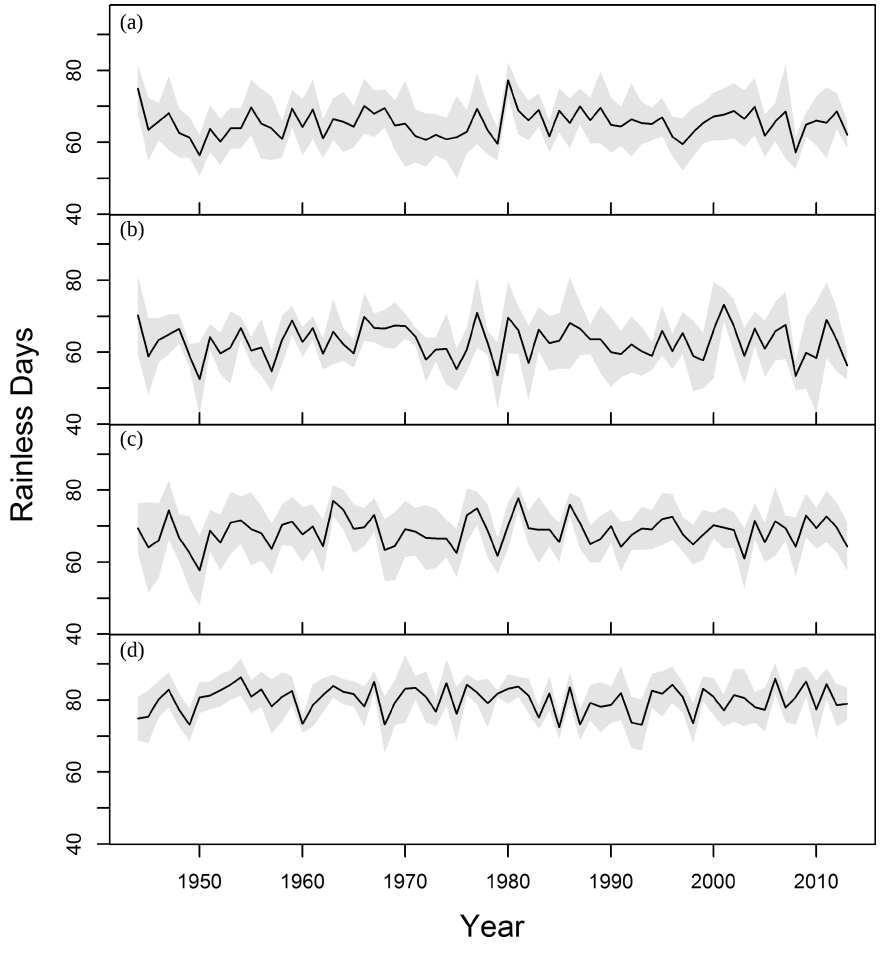

Figure S4. Mean **Winter** Rainless-day Frequencies (< 1 mm; Black Lines) for (a) Hudson Valley, (b) Ohio Valley, (c) Mississippi Valley, and (d) Southern Plains Regions with 95% Confidence Interval (gray shading) (1944–2013)

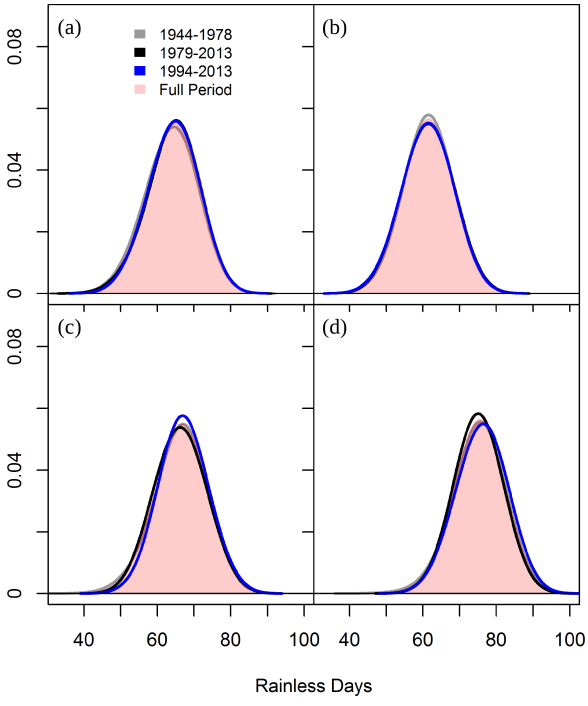

Figure S5. (Color online) Kernel Density Functions of **Spring** Rainless-day Frequencies ($<$ **1 mm**) for (a) Hudson Valley, (b) Ohio Valley, (c) Mississippi Valley, and (d) Southern Plains Regions. *Notes*: Kernel density functions computed for four distinct periods of time: 1944–1978 (gray line), 1979–2013 (black line), 1994–2013 (blue line), and the full period (1944–2013; transparent red shading).

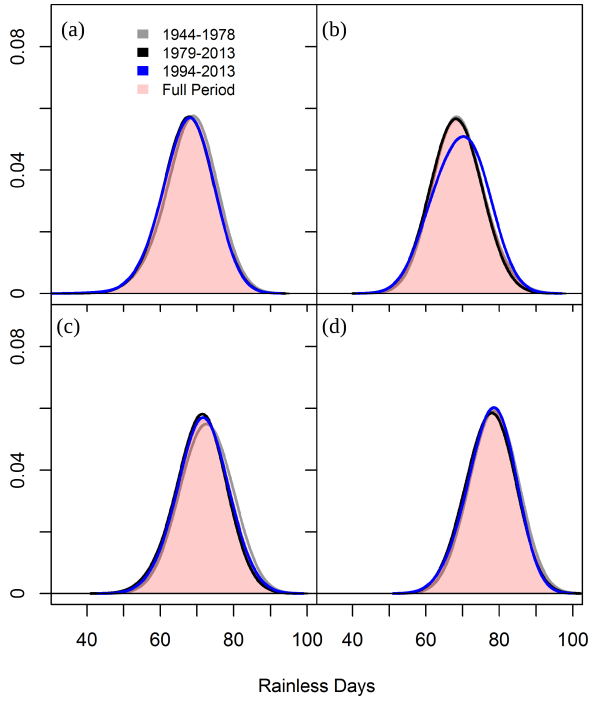

Figure S6. (Color online) Kernel Density Functions of **Fall** Rainless-day Frequencies ($<$ **1 mm**) for (a) Hudson Valley, (b) Ohio Valley, (c) Mississippi Valley, and (d) Southern Plains Regions.
Notes: Kernel density functions computed for four distinct periods of time: 1944–1978 (gray line), 1979–2013 (black line), 1994–2013 (blue line), and the full period (1944–2013; transparent red shading).

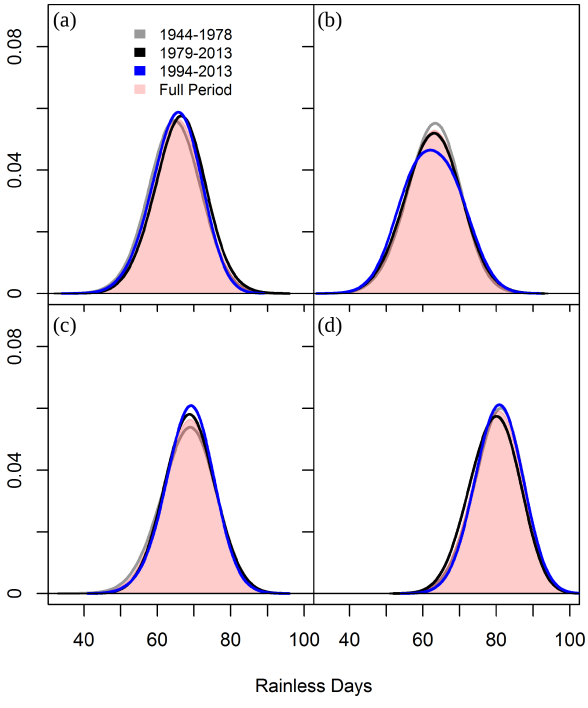

Figure S7. (Color online) Kernel Density Functions of **Winter** Rainless-day Frequencies (< **1 mm**) for (a) Hudson Valley, (b) Ohio Valley, (c) Mississippi Valley, and (d) Southern Plains Regions. *Notes*: Kernel density functions computed for four distinct periods of time: 1944–1978 (gray line), 1979–2013 (black line), 1994–2013 (blue line), and the full period (1944–2013; transparent red shading).

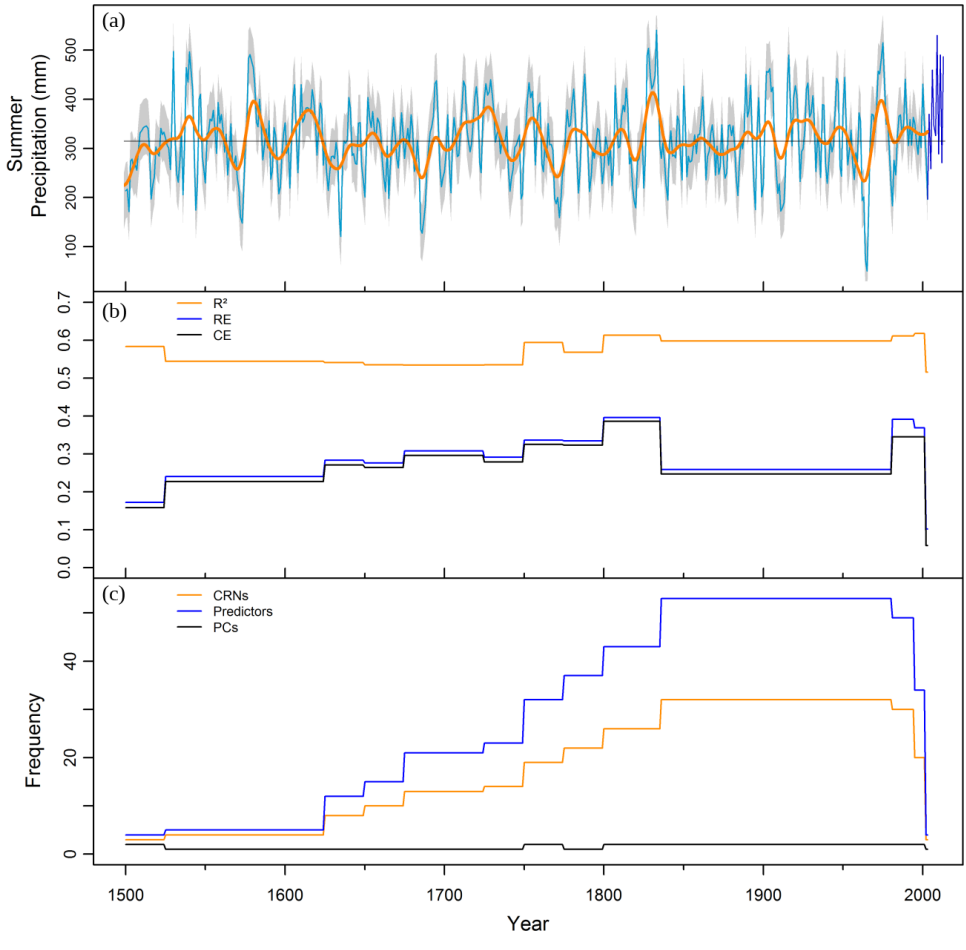

Figure S8. (Color online) Reconstructed Summer Precipitation in the Hudson Valley Region: (a) Precipitation Reconstruction (Light Blue) (1500–2003) with Instrumental Precipitation (Dark Blue) (2004–2013), 20-year Smoothing Spline (Orange) and Extrapolated RMSE (Light Gray Shade); and Model Calibration Statistics: (b) Coefficient of Determination (R^2; Orange), Reduction of Error (RE; Blue), and Coefficient of Efficiency (CE; Black), and (c) Sample Size of Predictors (Predict.; Blue), Chronologies (CRNs; Orange), and Principal Components (PCs; Black) of Summer Precipitation Reconstruction

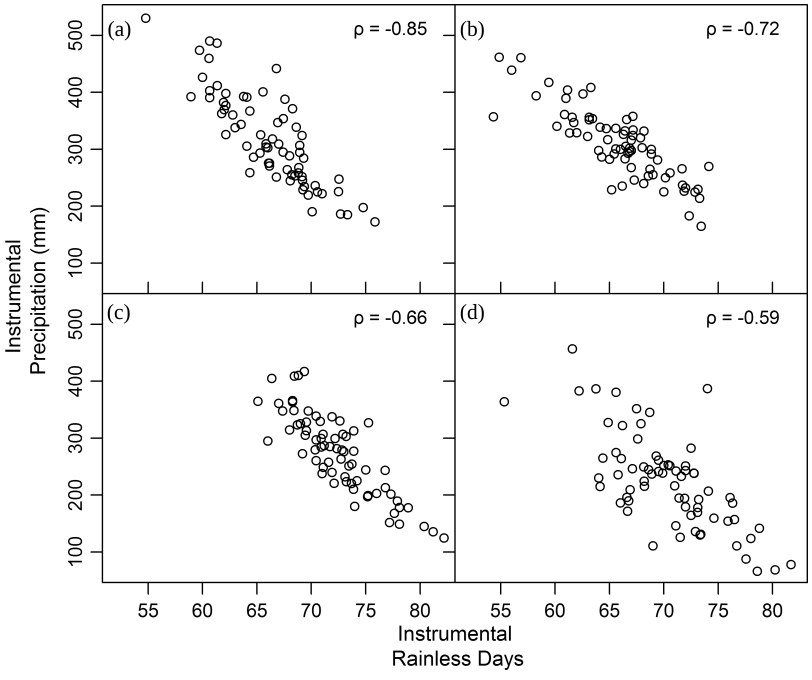

Figure S9. Scatterplot for Total Summer Instrumental Precipitation (*y*-axis) and Rainless Days (*x*-axis) (1944–2013) for (a) Hudson Valley, (b) Ohio Valley, (c) Mississippi Valley, and (d) Southern Plains Regions